

Bound states in the continuum in photonics

Kirill Koshelev,^{†,‡} Zarina Sadrieva,[†] Alexey Shcherbakov,[†] Yuri Kivshar,^{†,‡}
and Andrey Bogdanov^{*,†}

[†]*School of Physics and Engineering, ITMO University, 197101 St. Petersburg, Russian Federation*

[‡]*Nonlinear Physics Center, Research School of Physics, Australian National University,
Canberra ACT 2601, Australia*

E-mail: a.bogdanov@metalab.ifmo.ru

Abstract

Bound states in the continuum provide a remarkable example of how a simple problem solved about a century ago in quantum mechanics can drive the research on a whole spectrum of resonant phenomena in wave physics. Due to their huge radiative lifetime, bound states in the continuum have found multiple applications in various areas of physics devoted to wave processes, including hydrodynamics, atomic physics, and acoustics. In this review paper, we present a comprehensive description of bound states in the continuum and related effects, focusing mainly on photonic dielectric structures. We review the history of this area, basic physical mechanisms in the formation of bound states in the continuum, and specific examples of structures supporting such states. We also discuss their possible applications in optics, photonics, and radiophysics.

Introduction

One of the basic problems in quantum mechanics is the energy eigenvalue problem of a particle in a spherical quantum well. Below the barrier ($E < 0$), the spectrum is discrete and the wavefunctions $\psi(\mathbf{r})$ are bounded, i.e. $\int_{\mathcal{R}^3} \psi(\mathbf{r}) d\mathbf{r} < \infty$. Above the barrier ($E > 0$), the spectrum is continuous and the wavefunctions cannot be normalized in the classical sense [see Fig. 1(a)]. These solutions can be presented as propagating modes of the free space surrounding the quantum well. However, E. Wigner and J. von Neumann revealed in 1929 that this classification can be broken for specific potentials that asymptotically tend to zero away from the quantum well.¹ They showed that for some potentials, there are bound states embedded in the continuum of propagating modes [see Fig. 1(b)]. Today, such modes are known as *bound states in the continuum* (BICs). It seems that this term was introduced by L. Fonda in 1960.² We should mention that the work by E. Wigner and J. von Neumann contains an algebraic error that was mentioned and corrected by Stillenger and Herrick in Ref.³ Later, the theory of BICs was extended for the description of various atomic, molecular, and quantum mechanical systems,^{3–10} but the potential proposed by E. Wigner and J. von Neumann is rather specific and it has been never implemented. Some ideas on how to construct potentials supporting BIC in semiconductor superlattices were developed in Refs.^{11,12} However, they also were not implemented experimentally. We should mention that the experiment in¹³ has nothing in common with the observation of BICs in semiconductor superlattices. The Authors of this work simply observed a defect state in the bandgap spatially localized by electron Bragg reflectors. BICs are not a unique feature of quantum mechanical systems. In contrast, they are specific solutions of wave equations in general and they can exist in acoustics, hydrodynamics, aerodynamics,^{14–20} and optics.^{21,22} In acoustics and hydrodynamics, BICs have been known for a long time as *trapped modes*.^{19,23–25}

In recent years, BICs are actively studied in the areas of optics and photonics, as these states open up tremendous opportunities for implementing compact high-Q resonators and metasurfaces required for biosensing and enhancement of nonlinear optical effects and light-matter interaction. In the last few years, several reviews of the state-of-the-art achievements in BICs were published

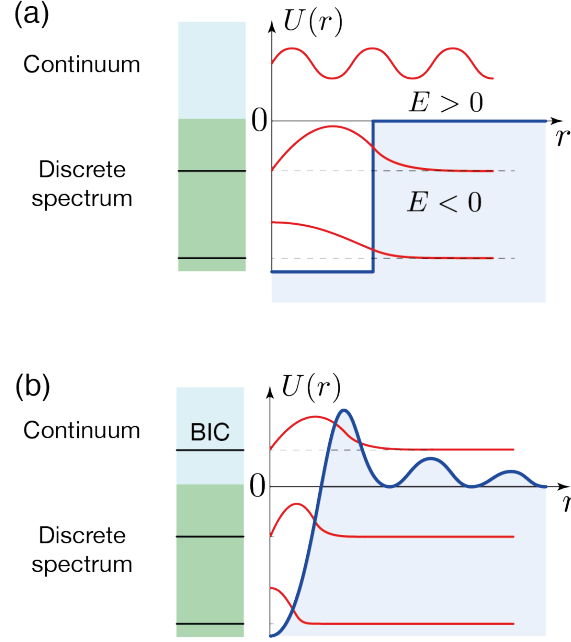


Figure 1: (a) Spherical quantum well: the spectrum is continuous for $E > 0$ and discrete for $E < 0$; (b) A specific potential results in the formation of bound states in the continuum

^{26–30}. In this review, we focus on BICs in electrodynamics systems in various spectral ranges, including visible, infrared, terahertz, and microwave ones. In this review, we present history, modern achievements, and different physical models explaining the nature of this beautiful phenomenon. In the first section, the history of BICs in optics is described, and a selection of pioneering scientific papers is presented, including those that were published before the introduction of the term ‘optical bound states in the continuum’. The second section is devoted to the description of various mechanisms of BICs formation in dielectric structures. Their quantum-mechanical nature, the importance and role of periodic potential for BICs implementation, and topological properties are discussed; an explanation of BICs properties in terms of multipole analysis is also provided. In the third section, examples of photonic structures with BICs are presented, and features of BICs are described in structures of various dimensionality: from single nanoparticles to periodic metasurfaces. In this section, we also briefly talk about quasi-BICs, which are formed from BICs due to the violation of symmetry of a photonic structure. In the fourth section, the applications of BICs are discussed for the detection of biological objects, laser generation, twisted light beams, and optical harmonics.

Historical reference

In modern literature, it is widely assumed that BICs in optical systems were predicted in 2008 in two works published by Marinica, Borisov, and Shabanov,²¹ and by Bulgakov and Sadreev,²² and that the first experimental study of BICs in optics was performed in 2011 in the work,³¹ where Marinica et al. considered two examples of similar periodic photonic structures supporting BICs. One of these structures is shown in Fig. 2(a). This is a two-layer dielectric grating periodic along the x -axis, and it has translational symmetry along the y -axis. The Authors showed that at certain distances between the gratings, the resonances in the reflection spectrum at oblique incidence become infinitely narrow, i.e. disappear from the spectra. They also mentioned that this state corresponds to the light perfectly propagating along the structure with no radiation losses. Bulgakov and Sadreev also considered a single-mode waveguide formed by two identical photonic crystals. They showed that light can be perfectly trapped at the defects of the photonic crystal despite the fact that the frequency of the trapped mode lies in the transmission band of the waveguide. Figure 2(b) shows the transmission spectra through the waveguide for different parameters of the defects (solid and dashed curves). The solid curve corresponds to the near-BIC case when Fano resonance collapses. The inset shows the field distribution at the minimum of the transmission.

Plotnik and colleagues performed a beautiful experiment on observation of the symmetry-protected BICs in a photonic structure that is an array of parallel dielectric single-mode waveguides fabricated of fused silica by direct laser writing [Fig. 2(c)].³¹ The near-field coupling between the waveguides results in the formation of a transmission band. Two additional waveguides fabricated above and below the array support the anti-symmetric mode with a frequency lying in the transmission band of the waveguide array. This anti-symmetric mode was excited from one side of the sample, and the intensity distribution was observed on the other side. The lower panel in Fig. 2(c) shows that the energy of the initial anti-symmetric mode does not leak to the waveguide array. In order to break the vertical symmetry, a gradient of the refractive index was created by heating the top side of the sample while cooling the bottom. Such heating results in the coupling of the excited anti-symmetric mode to the modes of the array. Thus, as the mode propagates through the sample,

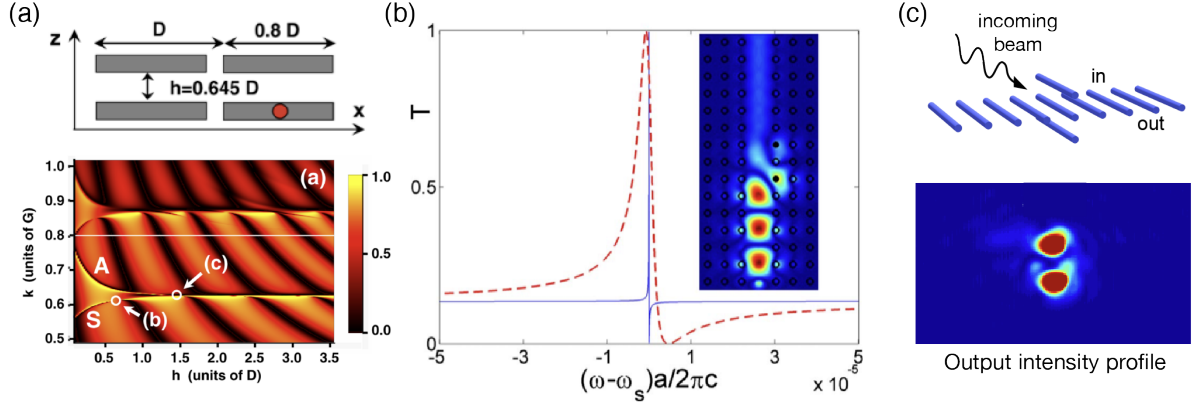


Figure 2: (a) Upper: schematic of a double grating structure in vacuum. Lower: specular reflection coefficient as a function of the wave vector k of the incident radiation and the distance h between the gratings for the fixed value of $k_x = 0.2G$. Adapted from Marinica et al.²¹ (b) The probability of transmission of a propagating photonic mode as a function of the frequency in the vicinity of the BIC for two sets of permittivity values. Inset: the mode profile. Adapted from Bulgakov et al.²² (c) Upper: schematic of a one-dimensional array of 51 and two additional waveguides above and below the array. Lower: light intensity at the output plane of the structure. Adapted from Plotnik et al.³¹

its energy is distributed between the waveguides forming the array. We would like to highlight that these three works revealed only the explicit connection between BICs in quantum mechanics and BICs optics for the first time. However, there are many earlier works where electromagnetic BICs were studied theoretically and experimentally but were not associated with quantum mechanics and the pioneering work by E. Wigner and J. von Neumann.

To the best of our knowledge, the history of BICs in optics began in 1976 with the work of Kazarinov, Sokolova, and Suris³² who considered a corrugated waveguide playing the role of a distributed-feedback resonator of a semiconductor laser. The Authors mentioned that if the eigenmode in the center of the Brillouin zone is formed by two counter-propagating waves which are π out of phase, then the radiation losses are canceled. Independently from this work, Vincent and Neviere considered theoretically the band structure of a dielectric corrugated waveguide [see Fig. 3(a)].³³ They showed that some resonances at the Γ -point of k -space are completely decoupled from the radiation continuum due to the symmetry mismatch between the mode and the external field, which leads to an infinite radiative lifetime of the mode. The authors of these works did not associate the observed resonances with BICs and they did not recognize the connection with earlier

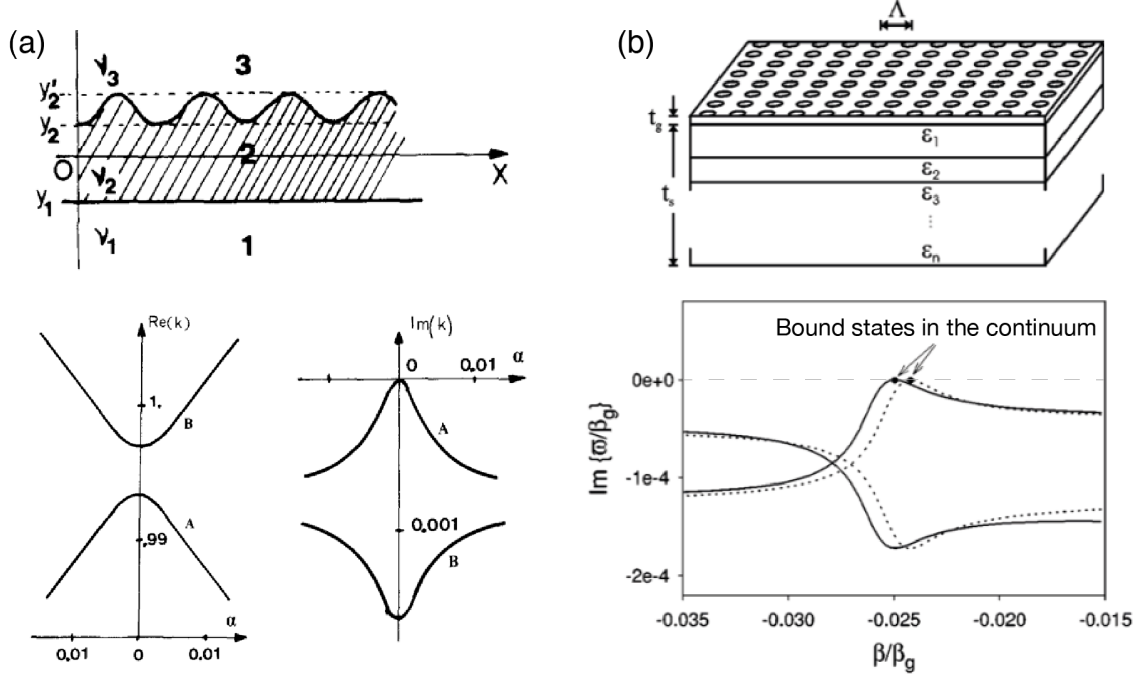


Figure 3: (a) Upper: Schematic representation of a corrugated waveguide. Lower: Dispersion curves for the normalized frequency. The curves correspond to the two distinct branches: the anti-symmetric one (A) and the symmetric one (B). Adapted from the work by Vincent and Neviere³⁴ (b) Upper: schematic of a multilayer slab waveguide with two-dimensional periodic texture. Lower: Imaginary part of frequency near the anti-crossing between TE-like and TM-like modes. The imaginary part of frequency turns to zero for the higher-energy band-edge states near the anti-crossing, indicating a truly bound state. Adapted from Paddon et al.³⁵

works in quantum mechanics, but the physics of non-radiating states were studied in detail.

Nonradiative states were also found in a two-dimensional periodic array of coupled dielectric spheres by M. Inoue and colleagues.³⁶ They showed that at the center of the Brillouin zone, optically inactive states exist that cannot be excited by a normally incident wave, regardless of its polarization. At the same time, they can be excited at oblique incidence, and in this case, extremely narrow peaks appear in the reflection/transmission spectrum, see Fig. 4(a). The existence of non-radiating modes in photonic crystal structures was also discussed by K. Sakoda^{37,38} and later by P. Paddon and J. Young.³⁵ The latter have developed a method based on Green's functions that allows analyzing a complex photonic band structure, i.e. the spectral positions of resonances and their radiative lifetimes [see Fig. 3(b)]. This is probably the first work where BICs with a non-zero Bloch wavenumber, the so-called parametric (tunable) BICs or accidental BICs, were theoretically

predicted. The authors explained that the coupling between the TE and TM modes leads to the anti-crossing of their dispersion curves and the formation of a mode with zero imaginary part of its eigenfrequency, i.e., the formation of BIC. In fact, the described mechanism is identical to that analyzed in the work of H. Friedrich and D. Wintgen for quantum mechanical systems.⁷ Therefore, tunable BICs are also called Friedrich-Wintgen BICs. In 2003, S. Shipman and S. Venakides also observed BICs numerically in the transmission spectra through an array of parallel dielectric cylinders [Fig. 4(b)]. In the same year, they developed a theory explaining the formation of bound states and anomalies in the transmission spectrum corresponding to these states.³⁹ Figure 4(b) (bottom panel) shows the numerical transmission spectrum for various Bloch wave numbers. It is explicitly shown that at normal incidence, a collapse of the Fano resonance occurs. The inset in the middle part of the figure shows the electric field distribution of the bound state. In fact, it is anti-symmetric with respect to the plane of symmetry of the unit cell; however, the authors plotted the distribution amplitude, which is an even function. In 2003, Bonnet et al.⁴⁰ discovered ultra-narrowband resonant reflection from a one-dimensional corrugated waveguide at oblique incidence, i.e. at non-zero Bloch wave number, and analyzed the effect of a finite beam size on the reflection spectrum.

It seems that the BICs were observed in experiment for the first time in the work by Henry et al in 1985.⁴² The Authors considered distributed-feedback resonator with a second-order grating. They showed that the losses of the lasing mode mainly occur at the ends of the structure, while at its center they nearly vanish due to the destructive interference of the scattered radiation from the counter-propagating waves forming the lasing mode, as it was predicted in the work³². Later on, in 1986,⁴³ Avrutskii et al. analyzed the reflectance spectra from the corrugated ZnO waveguide deposited on a glass substrate in the visible range. It was found that a peak in the second stop band disappears from the spectrum at the normal incidence, manifesting the bound state formed by counter-propagating waveguide modes.

Another experiment was done by Robertson and coauthors in 1992.⁴⁴ They analyzed the transmission spectra of a two-dimensional dielectric structure consisting of alumina-ceramic cylinders arranged in a square array. The experiment was performed in the GHz frequency range (10-150

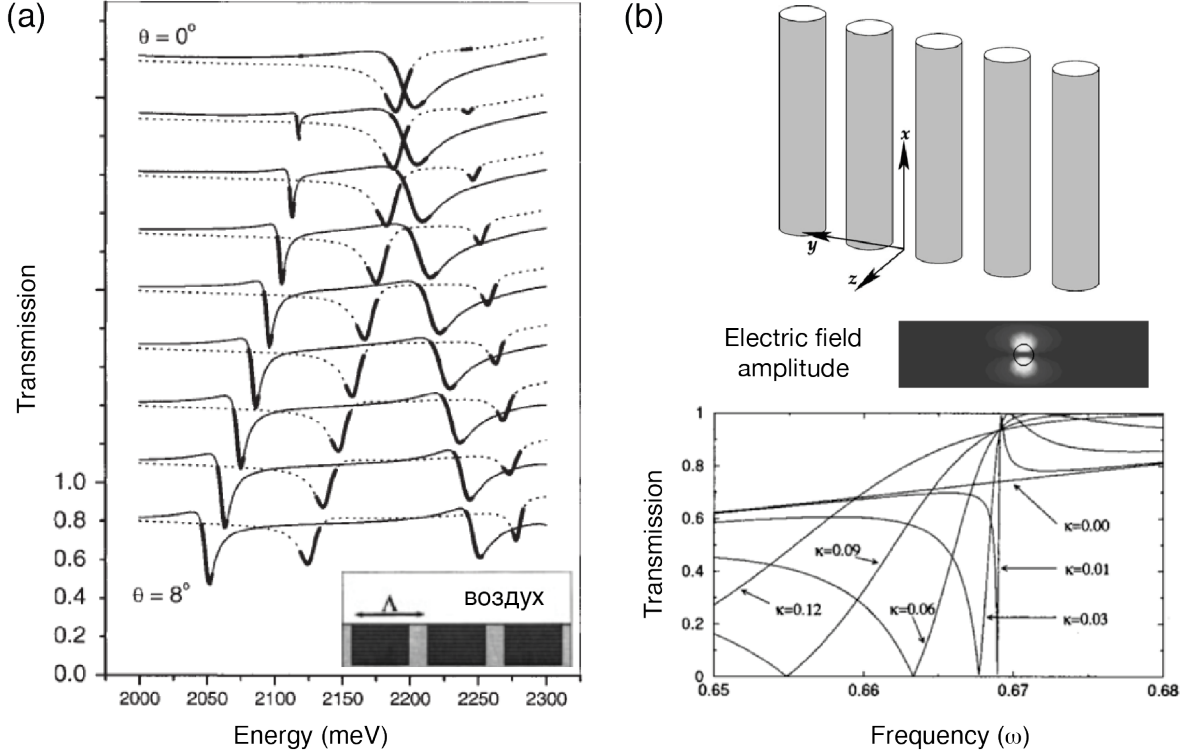


Figure 4: (a) The transmission spectra of a polaritonic crystal slab shown in the inset. The spectra are calculated for different angles of incidence, in the narrow energy interval around the fourth Bragg resonance of the lower polaritonic branch. line: the incident wave is polarized along the grooves (s-polarisation). Dotted line: the incident wave is polarized ortogonal to the grooves (p-polarisation). Adapted from Yablonskii et al.⁴¹ (b) Upper panel: schematic of a two-dimensional multilayer periodic slab. Middle panel: amplitude of the field of the bound state at $\kappa = 0$. Lower panel: Results of the numerical simulation using boundary integral equations of transmission vs normalized frequency for TE-polarized plane wave incident on a slab of vertical rods in air for various values of y component of the wave vector. The permittivity of the cylinders is 12, and the magnetic permeability is 1. Adapted from Shipman et al.³⁹

GHz). The Authors mentioned that one of the bands was not observed in the experiment because of the symmetry mismatch between the eigenmode and the exciting field. An experiment on the observation of BIC in the visible range was made in⁴⁵ by Pacradouni and colleagues. They measured the reflection spectra with angular resolution from the perforated AlGaAs membrane, confirming the narrowing lines in the vicinity of both at- Γ BIC (at normal incidence) and off- Γ BIC (at oblique incidence). However, we should note that this work contains a minor inaccuracy. Specifically, the existence of BICs with non-zero Bloch wave vector requires up-down mirror symmetry⁴⁶ or a very fine adjustment of the geometric and material parameters of the system,⁴⁷

which were not performed, according to the article. Thus, Pacradouni and colleagues observed only the increase of the Q factor, but not a BIC. For observation of off- Γ BIC, i.e. with a non-zero Bloch vector, in photonic crystal membranes, the structure is usually suspended⁴⁸ or covered by an optical liquid whose refractive index matches that of the substrate,⁴⁹ which provides the up-down mirror symmetry. The at- Γ BIC was also observed experimentally in a polaritonic system in 1998, by Fujita and colleagues.⁵⁰ The Authors analyzed the angular-resolved transmission spectra of a distributed-feedback microcavity consisting of quartz grating substrate covered by an organic-inorganic perovskite-type semiconductor. They discovered that at normal incidence the resonances disappear. These experimental results were comprehensively described by Yablonskii and colleagues in.⁵¹

In this section, we tried to review the key works on BICs in electromagnetic systems. However, we should note that the existence of non-radiating states in photonic structures was also discussed in many other works (see, for example, Refs.^{43,52–54}). To conclude this historical summary, we should mention that the physics of non-radiating states in periodic structures is quite clear, and other earlier works might exist where such states are discussed.

BICs in dielectric photonic structures

From quantum mechanics to photonics

Let us set a link between quantum mechanics and optics by the example of a 1D quantum well with a translational symmetry along the z -direction. For such a system, we can define the domain of the continuum spectrum as $\tilde{E} = E - \frac{\hbar^2 k_z^2}{2m} > 0$ [see Figure 5, left panel]. An optical analogue of this system is a parallel-plate dielectric waveguide. By rewriting the Helmholtz equation to the form of the stationary Schrödinger equation [see Figure 5, right panel], one can see that the permittivity $\varepsilon(x)$ can be associated with quantum mechanical potential $U(x)$. The waveguide modes lying under the light line $\omega < ck_z$ represent discrete states and all the modes with $\omega > ck_z$ form the continuum. Thus, in the system with a translational symmetry or periodicity along a

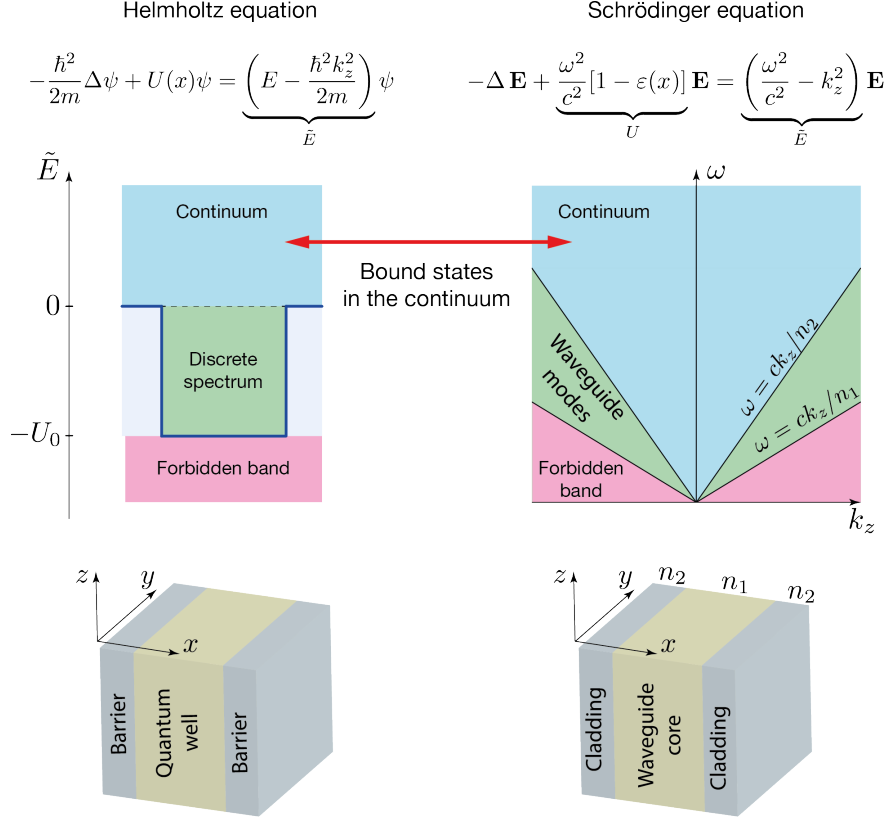


Figure 5: Correspondence between quantum mechanical and electromagnetic problems for an 1D potential having a translational symmetry along the z -direction. Upper panels: Schrödinger equation for 1D quantum well, and Helmholtz equation for a plane dielectric waveguide. Middle panels: potential well (left) and the dispersion diagram (right). Lower panels: potential well (left) and planar waveguide (right) in the coordinate space.

certain direction, BICs will be localized only in the orthogonal directions. The analogy between quantum and optical systems is very illustrative, but it is not complete. The vector structure of electromagnetic fields (polarization) makes the electromagnetic systems more diverse. We should also note that the Helmholtz equation written in the form of the stationary Schrödinger equation (Fig. 5) is a so-called generalized eigenvalue problem, since the required frequency ω is included both in the eigenvalue (the right side of the equation) and in the potential. However, if we consider the wave vector k_z as an eigenvalue, then we obtain a classical eigenvalue problem.

One of the general principles that can explain the appearance of BICs in most electromagnetic systems is the destructive interference of two interacting leaky waves. This mechanism was originally proposed by Friedrich and Wintgen,⁷ and it is schematically shown in Fig. 6(a). Let

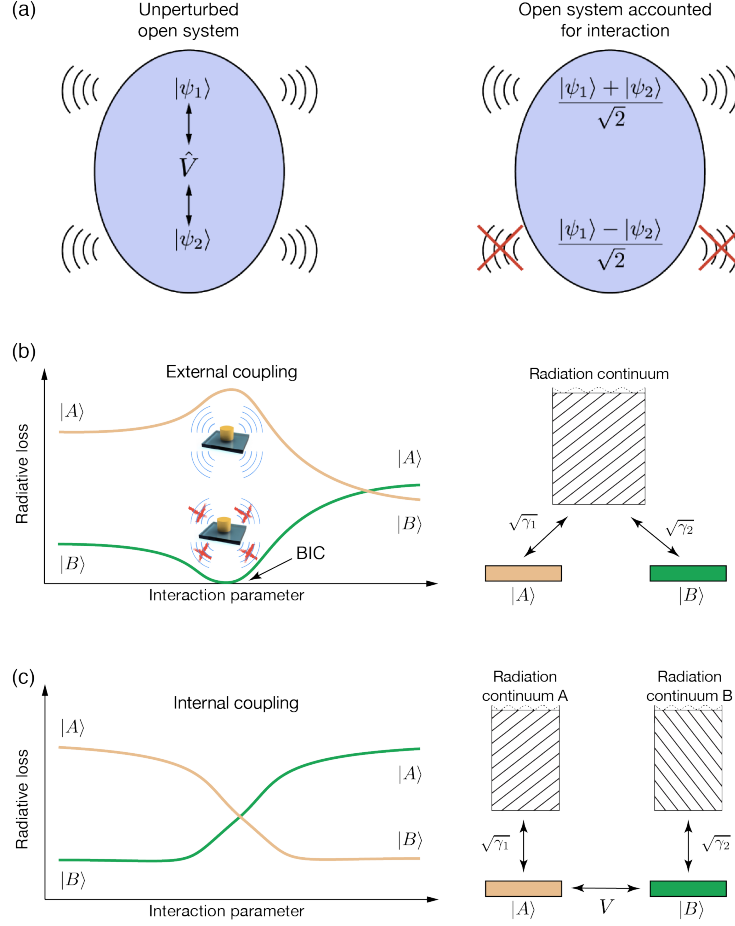


Figure 6: Illustration of the general principle explaining BICs proposed by Friedrich and Wintgen: (a) nonperturbed and perturbed open systems; (b) open system with two interacting leaky modes coupled to the same continuum, which allows for an existence of BIC; (c) open system with two interacting leaky modes coupled to different radiative continua, no BIC is allowed.

an open system (resonator) has two leaky modes $|\psi_s\rangle$ ($s = 1, 2$) with close or even equal eigenfrequencies $\Omega_s = \omega_s + i\gamma_s$ ($s = 1, 2$). Then, let's introduce some perturbation \hat{V} that makes these states coupled. In the framework of the perturbation theory, the eigenmodes in the system, with account for the interaction, can be presented as a linear superposition of the initial states $|\psi\rangle = C_1 |\psi_1\rangle + C_2 |\psi_2\rangle$. If we can continuously tune the interaction potential \hat{V} , then at some specific conditions, the radiative losses can be suppressed completely (substantially). In this case, a genuine BIC (or a quasi-BIC) appears.

More formally, an open system within the two-mode approximation can be described in the

framework of the temporal coupled-mode theory, where $\mathbf{a} = [a_1(t), a_2(t)]^T$ are the complex amplitudes of states $|\psi_1\rangle$ and $|\psi_2\rangle$. The complex amplitudes evolve in time as:

$$\frac{d\mathbf{a}}{dt} = \hat{H}\mathbf{a}, \quad (1)$$

$$\hat{H} = \underbrace{\begin{pmatrix} \omega_1 & \kappa \\ \kappa & \omega_2 \end{pmatrix}}_{\hat{H}_0} - i \underbrace{\begin{pmatrix} \gamma_1 & \sqrt{\gamma_1\gamma_2}e^{i\phi} \\ \sqrt{\gamma_1\gamma_2}e^{i\phi} & \gamma_2 \end{pmatrix}}_{\hat{V}}. \quad (2)$$

Here, κ is responsible for the internal coupling, $\sqrt{\gamma_1\gamma_2}$ accounts for the coupling through the radiation continuum, and ϕ is the phase shift between the modes. The condition of the BIC appearance in the two-mode approximation can be written as⁵⁵

$$\kappa(\gamma_1 - \gamma_2) = e^{i\phi}\sqrt{\gamma_1\gamma_2}(\omega_1 - \omega_2) \quad (3)$$

$$\phi = \pi m, \text{ where } m \in \mathbb{Z} \quad (4)$$

These conditions can be fulfilled through the tuning of the parameters of two coupled resonances. Figure 6(b) shows schematically how the radiative losses of the resonant states $|\psi_1\rangle$ and $|\psi_2\rangle$ depend on the coupling strength κ . It is worth mentioning that exactly at the point where the BIC appears, the radiative losses for the second mode are equal to $\gamma_1 + \gamma_2$. This is an analogue of the Dicke superradiance for two emitters.^{56,57}

In the framework of this simple model, the initial resonant states should radiate to the same radiative continuum (scattering channel). Only in this case they can interfere destructively and form a BIC. If the states $|\psi_1\rangle$ and $|\psi_2\rangle$ radiate to different radiative continua [see Fig. 6(c)], then the radiative losses of the dressed states will be always between γ_1 and γ_2 .⁵⁸

Now, let us illustrate how this model explains the formation of BICs in a corrugated dielectric waveguide. First, let's consider a periodic potential with a vanishing amplitude [see Fig. 7(a)]. This is the so-called empty lattice approximation, which is well-known in solid state physics⁵⁹. Therefore, the second bandgap is closed, and the eigenstates in the Γ -point are degenerate. They

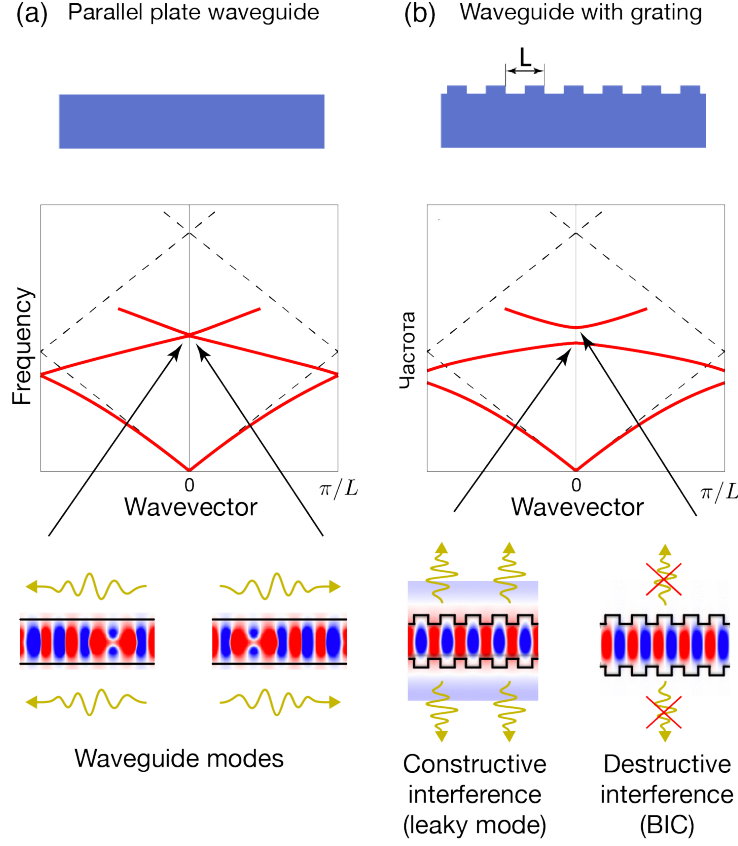


Figure 7: (a) Geometry, folded band structure and mode profiles for a dielectric waveguide. The waveguide supports guided modes propagating to the left and right. (b) Geometry, folded band structure and mode profiles for a modulated dielectric waveguide with period L . Due to the periodicity, the waveguide modes interact and form two new states due to constructive (leaky mode) and destructive (BIC) interference.

are counter-propagating leaky waves. Periodic potential with a finite amplitude lifts the degeneracy and opens the bandgap. If the periodic potential is symmetric with respect to the $z \rightarrow -z$ transformation, then the new states at the edges of the second bandgap are a BIC (anti-symmetric combination of the leaky modes) and a superradiant state (symmetric combination of the leaky modes) [see Fig. 7(b)]. This mechanism of BIC formation is quite clear, and it was discussed in many works, for example, in Refs.^{32,33,60,61}

BIC and diffraction orders

A BIC can be formed from a leaky resonance if the scattering amplitudes to all the channels turn to zero, i.e. in the case of decoupling from all the open scattering channels. This can be achieved by varying parameters of the system. In this case, the BIC formation is possible only if the number of the adjusted parameters is larger than the number of the scattering channels. For finite-size structures, the number of scattering channels is infinite, and the existence of BICs in such systems is prohibited by the non-existence theorem.²⁶ Until recently, it was believed that the only exception is the structures surrounded by a completely opaque shell providing the decoupling of the internal resonances from the outside radiation continuum, which in quantum mechanics corresponds to an infinite potential barrier, in acoustics to hard-wall boundaries, and in optics to perfectly conducting walls or epsilon-near-zero barriers.^{62,63} One more exception from the 'non-existence' theorem was found in,⁶⁴ where the authors revealed that finite-size solid acoustic resonators can support genuine BICs completely localized inside the resonator. Despite possible exceptions from the 'non-existence' theorem, the BICs are usually formed in structures with a finite number of scattering channels. A typical example of such a system is a resonator coupled to one or several waveguide modes^{20,65,66} or infinite photonic structures periodic in one or two directions.^{21,46,49,67,68}

Now, let us consider in more detail the mechanism of the BIC formation in periodic structures, by the example of a dielectric grating with a period L shown in Fig. 8(a). The electric field, being a Bloch function, can be written as

$$\mathbf{E}_{n,k_b}(x, y, z) = e^{ik_b z + ik_y y} \mathbf{u}_{n,k_b}(x, z). \quad (5)$$

Here, k_b is the Bloch wavenumber, k_y is the wavenumber component along the y -axis (the direction of the translational symmetry), and n is the index of the photonic band. Periodic function $\mathbf{u}_{n,k_b}(x, z)$ can be expanded into the Fourier series

$$\mathbf{u}_{n,k_b}(x, z) = \sum_s \mathbf{c}_{n,s}(x) e^{ik_b z + \frac{2\pi i s}{L} z}. \quad (6)$$

Here, s is an integer. Each term in this series corresponds to a diffraction channel, which could be open or closed. Outside the structure, the expansion coefficients describe a plane wave as

$$\mathbf{c}_{n,s}(x) \longrightarrow \mathbf{c}_{n,s} e^{\pm i K_s x}, \quad (7)$$

$$K_s = \sqrt{\frac{\omega^2}{c^2} - k_y^2 - \left(k_b^2 + \frac{2\pi s}{L}\right)^2}. \quad (8)$$

If K_s is real, then the diffraction channel is open and $\mathbf{c}_{n,s}$ is the complex amplitude of the wave outgoing via the s -th diffraction channel. If K_s is imaginary, then the diffraction channel is closed and $\mathbf{c}_{n,s}$ is the complex amplitude of the near field.

Figure 8(b) shows schematically the characteristic dispersion (ω vs k_b for $k_y = 0$) of eigenmodes in the dielectric grating. The colored domains in the figure show the regions where a certain number of diffraction channels (N) are open. Under the light line, $N = 0$. Thus, all the diffraction channels are closed, and only the waveguide modes exist in the structure.

To construct a BIC, all the coefficients $\mathbf{c}_{n,s}$ corresponding to the open diffraction channels should be equal to zero. However, for subwavelength structures with $L < \lambda$, there is only one open diffraction channel ($N = 1$) corresponding to $s = 0$. Thus, in order to form a BIC, we need to nullify $\mathbf{c}_0(x)$. Here, we omit the index n for the sake of simplicity. The function $\mathbf{c}_0(x)$ is the zeroth Fourier coefficient in the expansion (6), Thus, according to the definition

$$\mathbf{c}_0(x) = \int_{-L/2}^{L/2} \mathbf{u}_{k_b}(x, z) e^{-ik_b z} dz. \quad (9)$$

For the state in the center of Brillouin zone ($k_b = 0$) one can write

$$\mathbf{c}_0(x) = \int_{-L/2}^{L/2} \mathbf{u}_{k_b}(x, z) dz = \langle \mathbf{u}_{k_b}(x, z) \rangle_z. \quad (10)$$

Therefore, for BIC in the Γ -point, the z -averaged field should be equal to zero. If the unit cell of the grating is symmetric with respect to the $z \rightarrow -z$ transformation, then the eigenstates in the Γ -point

can be even or odd functions of z . For odd functions, their z -averaged value is zero. Therefore, all such states are BICs. These BICs are called *symmetry-protected*, which means that the cancellation of radiation is protected by the symmetry of the structure. It is noteworthy that symmetry-protected BICs emerge in both low-contrast and high-contrast photonic structures.^{61,69,70} As opposed to symmetry-protected BIC, there are the so-called Friedrich-Wintgen BICs, also known as *accidental* or *tunable* BICs, for which $c_0(x)$ nullifies not because of the symmetry reasons but due to the tuning of parameters of the system.^{46,49}

In the general case, the Fourier amplitude c_0 is a complex vector function of the grating parameters. Thus, for BIC formation, both its real and imaginary parts should be zero. However, one can show that for BIC, the components of c_0 can be chosen real everywhere in the k -space if the structure possesses time-reversal symmetry $\varepsilon^*(\mathbf{r}) = \varepsilon(\mathbf{r})$, inversion symmetry $\varepsilon(-\mathbf{r}) = \varepsilon(\mathbf{r})$, and up-down mirror symmetry.^{46,49} However, a symmetry-protected BIC does not require up-down mirror symmetry, and therefore it can be implemented in structures with substrate. This symmetry is necessary for observation of a tunable (off- Γ) BIC. Thus, as it was mentioned above, in experiments the samples are usually immersed in an optical liquid that is index-matched to the substrate, or suspended structures are used.^{49,71}

In order to create a BIC, it is not necessary to work in a region with only one open diffraction channel. If several diffraction channels are open, one needs to tune several parameters of the system to achieve a BIC. It is hard to implement in practice, but there are theoretical works showing it is possible.^{72,73}

BICs and the multipole expansion

The appearance of BICs in periodic photonic structures can be explained in terms of the multipole expansion. The multipole approach is based on the formalism of the vector spherical harmonics (multipoles) representing a complete basis set of orthogonal vector functions that are the solutions of the vector Helmholtz equation.⁷⁴ Usually, these functions are used in the Mie theory as independent scattering channels. They give the connection between the directivity diagram of the

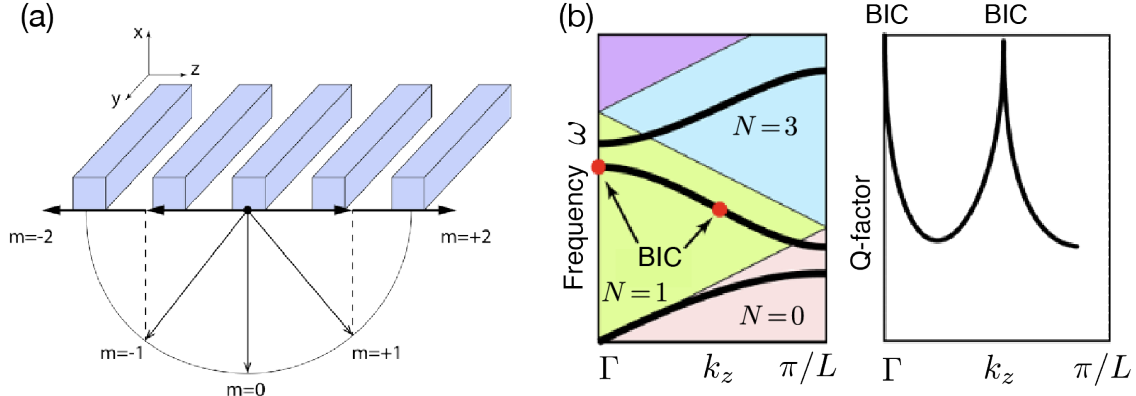


Figure 8: (a) Example of a 1D dielectric grating; (b) typical dispersion for 1D grating, where colors indicate the domains with different numbers of diffraction channels, and the dots indicate the positions of BICs (left); variation of the Q factor along the second dispersion curve (right).

outgoing radiation and the polarization currents induced inside a scatterer by the incident wave.⁷⁵ A number of beautiful scattering phenomena in the area of electromagnetic waves were explained within the multipole approach including the anapole effect,^{76,77} the Kerker effect,^{78–80} and super-scattering.^{81–84} The multipole approach can also enable a deeper understanding of the physics of BICs in periodic structures.^{85,86}

Following the book by Bohren and Huffman,⁸⁷ we define the vector spherical harmonics $\mathbf{M}_{p\ell m}$ and $\mathbf{N}_{p\ell m}$ as

$$\mathbf{M}_{p\ell m} = \nabla \times (\mathbf{r}\psi_{p\ell m}), \quad p = o, e \quad (11)$$

$$\mathbf{N}_{p\ell m} = \frac{1}{k} \nabla \times \nabla \times (\mathbf{r}\psi_{p\ell m}), \quad p = o, e \quad (12)$$

$$\psi_{\{o\}}^e_{\ell m} = z_\ell(kr) P_\ell^m(\cos \theta) \begin{cases} \cos m\varphi \\ \sin m\varphi \end{cases}. \quad (13)$$

Here, $\{r, \theta, \varphi\}$ are spherical coordinates, P_ℓ^m is an associated Legendre polynomial, $z_\ell(kr)$ is a spherical Bessel function describing the incoming, outgoing, or standing wave, $\ell = 1, 2, 3, \dots$ is the total angular momentum quantum number, $m = 0, 1, \dots, \ell$ is the absolute value of the projection

of the angular momentum (magnetic quantum number), and k is the wavenumber in vacuum or medium depending on the considered domain of the space. For brevity, we introduce $\mathbf{W}_j = \{\mathbf{M}_{p\ell m}, \mathbf{N}_{p\ell m}\}$, where $j = \{p, \ell, m\}$. Let us consider an eigenmode of a photonic crystal slab or a metasurface [see Fig. 9(a)]. The electric field of the mode outside the structure can be represented as

$$\mathbf{E}(\mathbf{r}) = \sum_{\mathbf{K}_s, j} D_j \int_{-\infty}^{+\infty} d\mathbf{k}_{\parallel} \frac{e^{i\mathbf{k}\mathbf{r}}}{k_z} \mathbf{Y}_j \left(\frac{\mathbf{k}}{|\mathbf{k}|} \right) \delta(\mathbf{k}_b - \mathbf{K}_s - \mathbf{k}_{\parallel}). \quad (14)$$

Here, \mathbf{Y}_j is the Fourier transform of \mathbf{W}_j , \mathbf{k}_b is the Bloch wavenumber, \mathbf{K}_s is the reciprocal lattice vector, D_j is the amplitude corresponding to \mathbf{Y}_j . The coefficient of the expansion of the far field D_j is directly connected with the expansion coefficient of the polarization inside the unit cell.⁸⁶

Equation (14) shows that the far field of the structure is defined by multipole content of the unit cell, but filtered by the open diffraction channels. **The BIC is formed if the directions of all the open diffraction channels coincide with the nodal lines of the unit cell.**

The simplest example is the subwavelength lattice of identical in-phase point dipoles oriented perpendicular to the lattice plane. Such a configuration corresponds to the mode with $\mathbf{k}_b = 0$, i.e. to the Γ -point. The only allowed direction of the diffraction is normal to the metasurface, however, dipoles do not radiate in the direction of their axis. Therefore, this mode does not radiate, being a symmetry-protected BIC.⁸⁸ It is shown in Ref.⁸⁶ that there are two scenarios of BICs in subwavelength structures [see Fig. 9(b)]. In the first scenario, all the multipoles contributing to the eigenmode do not radiate in the direction orthogonal to the structure. This corresponds to the symmetry-protected BIC. One can show that the multipoles $\mathbf{M}_{p\ell m}$ and $\mathbf{N}_{p\ell m}$ do not radiate up- and downwards if $m \neq 1$.^{85,86} Therefore, all the modes in the Γ -point not containing the multipoles with $m = 1$ are symmetry-protected BICs. In the second scenario, the interference from all the multipoles included in the mode suppresses the radiation in the direction of the open diffraction channel. This corresponds to the accidental BIC.

To find all the multipoles allowed for a certain mode, one can address to the group theory. Indeed, the eigenmodes are transformed by irreducible representations of the structure's symmetry

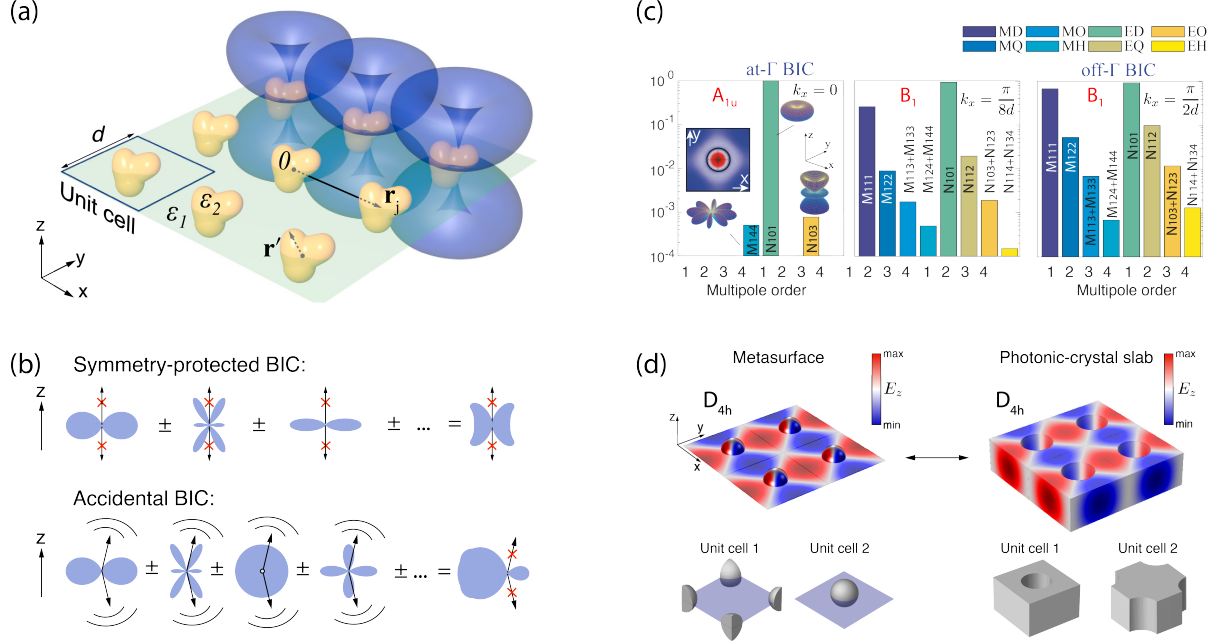


Figure 9: Multipole origin of the bound states in the continuum – (a) A periodic dielectric metasurface with square lattice. (b) Mechanisms of BICs formation. (c) Multipole decomposition of the TM-polarized eigenmode of the metasurface composed of dielectric spheres with $\varepsilon_2 = 12$ ($\varepsilon_1 = 1$). Each panel corresponds to particular Bloch wave vector k_x . The vertical axis shows the relative amplitude of electric and magnetic multipoles, and different orders n are indicated with different colors. The irreducible representations are marked by red. The inset in the first panel shows the E_z field profile in the central cross section. (d) Distribution of the E_z component of the electric field of the modes corresponding to the same irreducible representation B_{1u} in the photonic crystal slab and metasurface. The bottom panel illustrates the variants of the unit cells for which the multipole content is identical.

group.^{89–91} While the unit cell determines the point group symmetry, the Bloch functions form a basis of irreducible representation of the translation group. The symmetry group of a particular wave vector \mathbf{k}_b is defined as a subgroup of the whole point group that keeps the \mathbf{k}_b invariant. Studying the multipole content of the mode, first we should find the irreducible representation of the mode at the given \mathbf{k}_b . The set of multipoles in the decomposition is determined directly by the irreducible representation of the mode. Figure 9(c) shows the multipole content of the mode supported by a square array of dielectric spheres. The parameters of the structure are described in the caption. In the Γ point, \mathbf{k}_b -group coincides with the point-group symmetry of the unit cell. Out of the Γ point, the irreducible representation changes. Three main multipoles contributing to the symmetry-protected BIC in the considered example are shown in Fig. 9(c) (left panel). As we

mentioned previously, for the accidental BIC, the sum of the vector spherical harmonics (Eq. (14)) is nullified in the direction of the open diffraction channel. The multipole content of the accidental BIC is shown in the third panel in Fig. 9(c).

One can show that in the square lattice (D_{4h} , D_{4v}) all singlet states in the Γ -point with the frequency $\omega/c < 2\pi c/d$ are symmetry-protected BICs, while the bright modes are doubly degenerate.⁸⁶ However, in the triangular lattice (D_{6h} , D_{6v}), there are two two-dimensional representations. One of them does not contain the multipoles with $m = 1$. Therefore, such structures can host doubly-degenerate symmetry-protected BICs.⁹² Recently, Overvig and co-authors presented a quite detailed catalogue of the selection rules for symmetry-protected BICs in two-dimensional photonic crystal structures.⁹³

If the metasurface consists of meta-atoms characterized by a single multipole (dipole, quadrupole, octupole, etc), then the position of the accidental BIC in the k -space is determined by the direction of the nodal line of the multipole. Of course, the multipole approach is more natural for the metasurfaces consisting of resonant meta-atoms, but strictly speaking, it can be applied fairly for the photonic crystal slabs in the case of low-contrast materials or when the filling factor is low. As an example, Fig. 9(d) shows the field distribution for two modes of the same symmetry in a metasurface and a photonic crystal slab with D_{4h} symmetry.

BICs and topological charges

Usually, BICs are robust to the change of some parameters of the system – they do not disappear, but shift in the configuration space. Such robustness can have topological origin and, thus, can be characterized by topological invariants (topological charges). Here, we consider three illustrative examples of topological robustness of BIC in the configuration space. We have shown above that BICs appear in periodic structures when the vector Fourier amplitude responsible for the radiation to the open diffraction channels nullifies. It was shown in Ref.⁴⁶ that the polarization structure of the Fourier amplitude in the vicinity of a BIC forms a vortex that can be characterized by a topological charge showing the number of 2π rotations of the polarization vector around the BIC

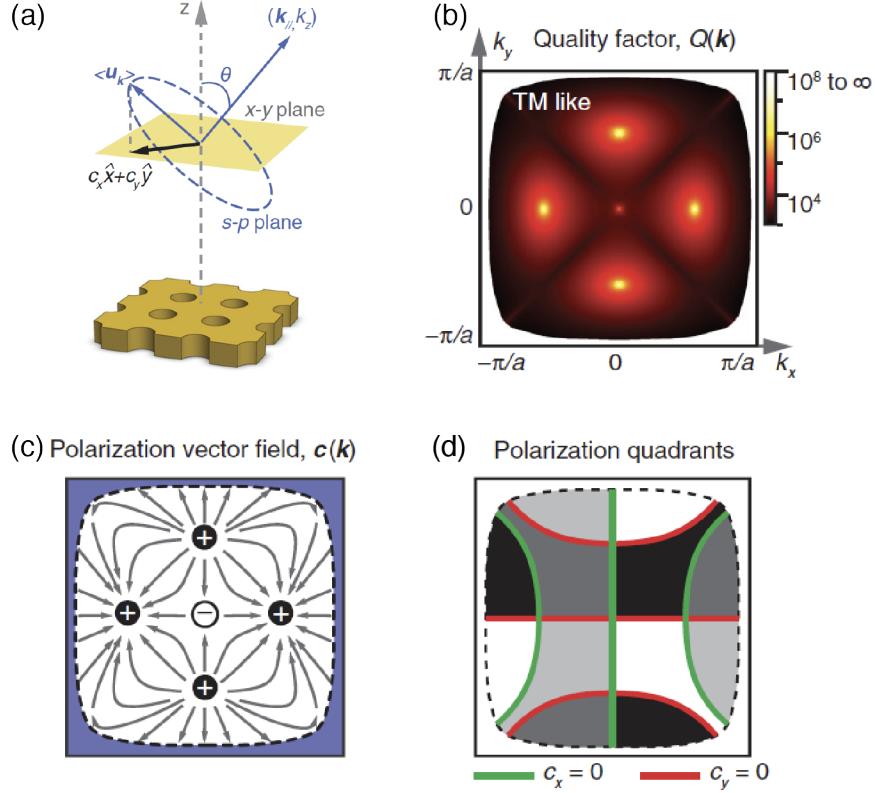


Figure 10: (a) Scheme of the expansion of the radiation field for the resonances of a photonic crystal plate. The spatially-averaged Bloch part of the electric field $\mathbf{c}(\mathbf{k}) = \langle \mathbf{u}_k \rangle$ is projected onto the xy plane as the polarization vector $\mathbf{c}(\mathbf{k}) = (c_x, c_y)$. Resonance turns into a BIC when $c_x = 0$ and $c_y = 0$. (b) Map of the radiative Q factor calculated for the TM_1 modes of a square-lattice photonic crystal slab in the first Brillouin zone. For the plotted mode, five BICs are visible: four accidental and one symmetry-protected. (c) Directions of the vector field of polarization show the vortices with topological charges $+1$ and -1 . The blue shaded area indicates the region below the light line. (d) Nodal lines of the components of the polarization vector $\mathbf{c}(\mathbf{k})$. Based on the work of Zhen et al.⁴⁶

in the reciprocal space.

According to the Bloch theorem, the electric field of a mode in photonic crystal slab [see Fig. 10(a)] can be written (similar to the case of 1D grating considered earlier) can be written as

$$\mathbf{E}_{\mathbf{k}}(\boldsymbol{\rho}, z) = e^{i\mathbf{k} \cdot \boldsymbol{\rho}} \mathbf{u}_{\mathbf{k}}(\boldsymbol{\rho}, z). \quad (15)$$

Here, $\mathbf{k} = (k_x, k_y, 0)$ is a two-dimensional two-dimensional Bloch wave vector, $\boldsymbol{\rho} = (x, y, 0)$ is a radius vector lying in the plane of the slab, and z is the normal direction to the slab. $\mathbf{u}_{\mathbf{k}}(\boldsymbol{\rho}, z)$ is a periodic function of $\boldsymbol{\rho}$. The zero-order Fourier amplitude $\mathbf{c}(\mathbf{k}) = \langle \mathbf{u}_{\mathbf{k}} \rangle$ defines the amplitude and polarization of the outgoing wave. The spatial average is taken over the unit cell in any horizontal plane outside the slab. Since the BIC radiates neither x nor y polarization, it appears in \mathbf{k} -space at the crossings of the line corresponding to $c_x(k_x, k_y) = 0$ and $c_y(k_x, k_y) = 0$ [see Figs. 10(b) and 10(d)]. The topological charge q characterizing the BIC can be introduced as follows

$$q = \frac{1}{2\pi} \oint_C d\mathbf{k} \cdot \nabla_{\mathbf{k}} \phi(\mathbf{k}), \quad q \in \mathbb{Z}. \quad (16)$$

Here $\phi(\mathbf{k}) = \arg [c_x(\mathbf{k}) + ic_y(\mathbf{k})]$, and C is a simple path in \mathbf{k} -space that goes around the BIC in the counter-clockwise direction. The polarization vector has to come back to itself after the closed loop, so the overall angle change must be an integer multiple of 2π , and, thus, q must be an integer. For the considered structure, the symmetry-protected BIC carries a charge of $q = +1$, see Fig. 10(c). The topological charge of BIC hosted by the silicon nitride grating was measured experimentally using the angle- and wavelength-resolved polarimetric reflectometry.⁹⁴ It was shown in Ref.⁴⁶ that the topological charge of BICs in gratings can be only $q = 0, \pm 1$. The topological charge in structures periodic in two dimensions can be arbitrary high. However, all designs of the photonic structures proposed up to date support BICs with a maximum value of the topological charge of $|q| = 2$.^{46,95} The observation of a BIC with a higher topological charge remains an unsolved challenge.

Being robust against changes in some geometrical parameters of the structures, the polarization

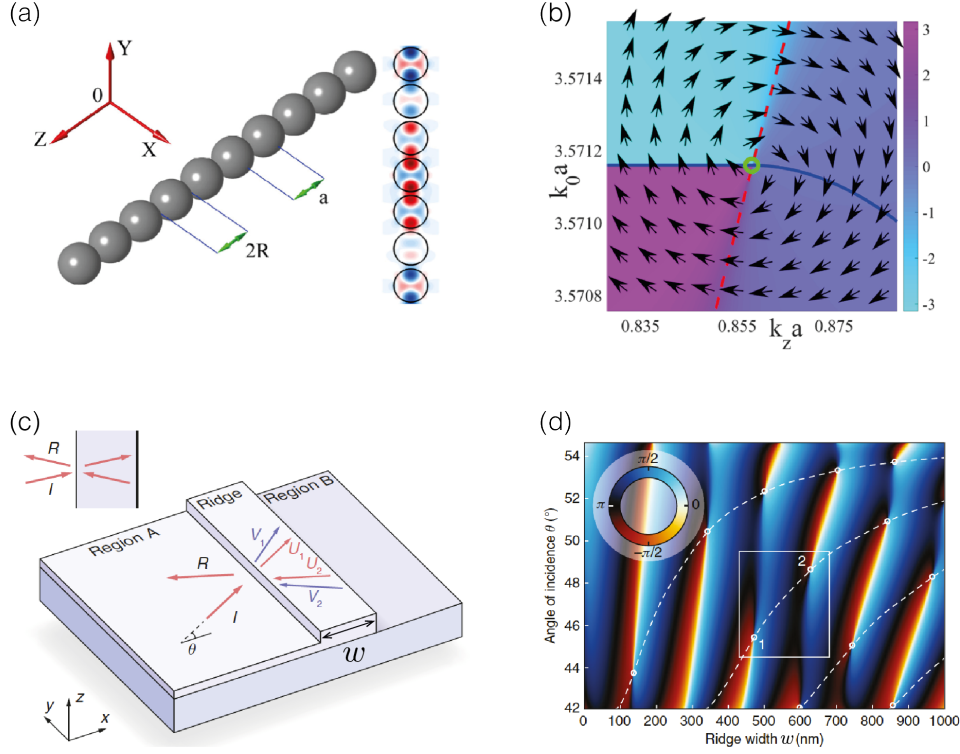


Figure 11: (a) Periodic array of dielectric spheres and the distribution of the magnetic field amplitude H_z for a BIC plotted in the $y0z$ plane. (b) Phase map of the coupling coefficient $W(\omega, k_z)$. The vectors show a vortex around a BIC. Adapted from Bulgakov et al.⁹⁶ (c) Schematic view of the on-chip analog of the Gires-Tournois interferometer supporting a BIC. (d) Phase map of the coupling coefficient $\mathcal{P}(w, \theta)$. Adapted from Bykov et al.⁹⁷

vortex can migrate inside the Brillouin zone over a dispersion surface. Within the given photonic branch, the total topological charge is conserved. It leads to restrictions on the behavior of BICs. For example, a BIC can be destroyed through the annihilation when two or several topological charges with total zero charge collide. A BIC with an integer topological charge can decay into several BICs with integer topological charges or into circularly polarized states with half-integer charges.^{46,95,98,99} Some examples of the topological charges' migration and decay will be considered in the section 'Dielectric Gratings'. The topological charge carried by a BIC can be used for the generation of optical vortex beams.^{100–102}

In Ref.,⁹⁶ the Authors developed quite a general approach for defining topological charge of BIC in a wide class of systems and then applied the developed formalism to linear periodic chains

of coupled resonators [Fig. 11(a)]. The Authors introduced a complex function $W(\omega, k_z)$ (quasi-mode coupling strength) characterizing the coupling efficiency between the scattering channel and the resonant states of the system. Here, k_z is the wavenumber of the incident wave and ω is its frequency. Function $W(\omega, k_z)$ can be interpreted as a projection of the incident wave onto the eigenmode, or which is the same, the projection of the resonant state onto the wave outgoing through the scattering channel. Obviously, $W(\omega, k_z) = 0$ for BIC, because the BIC appears in $\omega - k_z$ space exactly at the crossing of lines corresponding to $\text{Re}\{W(\omega, k_z)\} = f(\omega, k_z) = 0$ and $\text{Im}\{W(\omega, k_z)\} = g(\omega, k_z) = 0$. The topological charge q can be introduced as

$$q = \text{sgn} \left(\frac{\partial f}{\partial \omega} \frac{\partial g}{\partial k_z} - \frac{\partial g}{\partial \omega} \frac{\partial f}{\partial k_z} \right) \Big|_{\text{BIC}}. \quad (17)$$

Figure 11(b) shows the phase $\theta = \arg[W(\omega, k_z)]$. One can see that the gradient of the phase $\mathbf{j} = \nabla \theta$ forms a vortex around the BIC. Therefore, a BIC in the linear periodic chain can also be characterized by a topological charge. However, it is still an open question how to measure such a charge experimentally.

Another beautiful example of BIC was observed in the dielectric ridged waveguide forming an on-chip analog of the Gires-Tournois interferometer [see Fig. 11(c)].⁹⁷ The Authors showed that such a waveguide can support a BIC – the mode that does couple neither to waveguide modes in region A, nor to the propagating waves in the substrate and in air. This type of BIC was predicted and experimentally observed in the Refs.^{103–105} A rigorous theory proving that these states are BICs was developed by Bezus, Bykov, and Doskolovich.¹⁰⁶ Similar to Ref.,⁹⁶ they introduced a complex quasimode coupling $\mathcal{P}(w, \theta)$ between the modes of the ridge and waveguide modes in region A. If the frequency is fixed, then the BIC in the considered system can be observed at the specific values of angles θ and width of the ridge w . Exactly at the BIC, $\mathcal{P}(w, \theta)|_{\text{BIC}} = 0$, and its phase is singular (i.e. non-defined). The topological charge introduced as

$$q = \frac{1}{2\pi} \oint_{\gamma} \text{darg } \mathcal{P}(w, \theta) \quad (18)$$

can be equal to ± 1 . By variation of the waveguide layer thickness in region B, the Authors showed that the BICs can move in $w - \theta$ space and even annihilate, if two BICs with opposite charges collide. We should note that instead of varying w at a fixed frequency ω , one can vary ω at a fixed ridge width w . In this case, the results will be completely the same. To conclude, we should add that the topological charge can be introduced in many ways, but not all of the introduced charges will have a clear physical meaning, and thus, they cannot be directly measured in the experiment.

Losses and Q factor of quasi-BICs

Losses limit the total Q-factor Q_{tot} of BIC. In general, Q_{tot} can be decomposed into partial contributions:

$$Q_{\text{tot}}^{-1} = \underbrace{Q_{\text{rad}}^{-1} + Q_{\text{surf}}^{-1} + Q_{\text{str}}^{-1} + Q_{\text{size}}^{-1} + Q_{\text{subs}}^{-1}}_{\text{radiative}} + \underbrace{Q_{\text{abs}}^{-1}}_{\text{non-radiative}}. \quad (19)$$

Here, the radiative losses account for surface roughness (Q_{surf}), structural disorder (Q_{str}), diffraction losses due to finite size of the sample (Q_{size}), and diffraction into high-index substrate (Q_{subs}). The non-radiative losses Q_{abs} include all types of absorption (fundamental absorption, free-carrier absorption, multiphoton absorption, etc). The loss mechanisms in a periodic photonic structure are shown schemtically in Fig. 12(a). The statement that BICs have infinite Q factor is quite common in the literature, but it is not completely correct. Only the radiative Q factor diverges for BICs ($Q_{\text{rad}} \rightarrow \infty$), as they are completely decoupled from the radiative continuum, but the total Q factor can remain finite. For example, BICs with finite Q_{tot} can be observed in plasmonic structures, where the losses are essential.^{107–109}

Strictly speaking, BICs are a mathematical idealization, and unavoidable radiative losses turn them into *quasi-BICs*, which manifest themselves in the scattering spectra as sharp Fano resonances.¹¹⁰ Quasi-BICs are important for applications, as they are still strongly localized and provide a giant enhancement of the incident field, and they can be excited by an external incident wave. Usually, the efficient performance of photonic structures requires a critical coupling of the eigenmode to the incident field, which is achieved at the condition $Q_{\text{abs}} = Q_{\text{rad}}$.^{111–115} The absorption

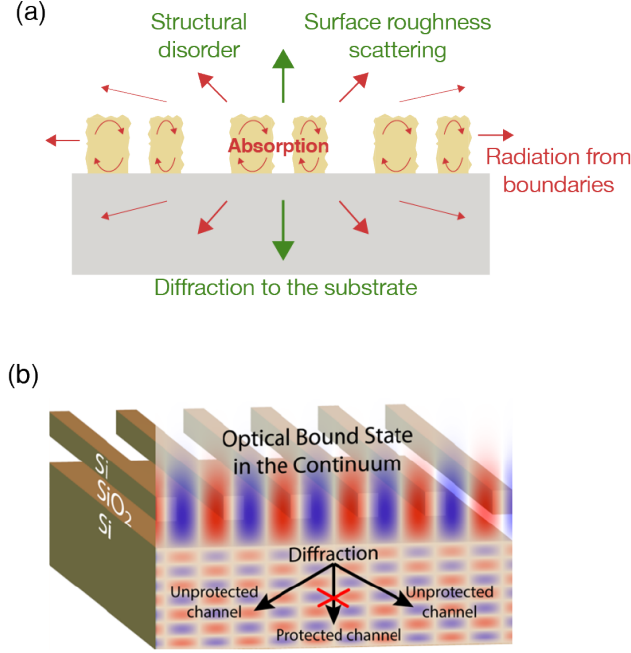


Figure 12: (a) Mechanisms of losses in a periodic photonic structure. They include surface roughness, radiative loss due to structural disorder, diffraction losses due to finite size of the sample, and diffraction to high-index substrate. (b) A symmetry-protected BIC in a grating etched on the silicon-on-insulator wafer. Diffraction that is normal to the surface plane is prohibited by the symmetry of the BIC, while diffraction into the substrate is allowed.

rate in semiconductors, for example, can be controlled in the visible, infrared, and terahertz ranges via free electrons induced by an external optical pulse.^{116–118} The radiative losses of quasi-BICs in periodic photonic structures can be controlled by the size of the sample,^{67,119,120} the angle of incidence⁴⁹ or asymmetry of the unit cell.¹¹⁰ It seems that the latter is the most precise and powerful technique, and thus, more suitable for applications requiring normal incidence excitation. The optical properties of the asymmetric photonic structures with quasi-BICs and their applications are discussed in the following Sections. Another mechanism of the dynamic all-optical control over the radiative losses of BICs was proposed in Ref.¹²¹ It was shown that the Kerr-type nonlinearity can result in radiative losses, which appear due to the coupling between the symmetry-protected BIC and a bright mode of the system. Thus, the radiative losses of BICs can be controlled by the intensity of the incident light. A similar mechanism of the radiative loss control was proposed for the implementation of optical memory based on BICs.^{122,123}

One of the loss mechanisms is the diffraction into the substrate with a high refractive index.

This mechanism is crucial, for example, for photonic structures fabricated from a silicon-on-insulator wafer.¹²⁴ In this case, the refractive index of the substrate is higher than the effective refractive index of the BIC, thus, there is a diffraction into the substrate [see Fig. 12(b)]. It is important that despite the presence of the substrate with a high refractive index, the zero-order diffraction into the substrate is closed for symmetry-protected BICs, as the substrate does not break C_2 symmetry with respect to the vertical axis. The intensity of the diffraction into the substrate strongly (exponentially) depends on the thickness of the SiO_2 buffer layer isolating the photonic structure from the substrate. Thus, Q_{tot} increases with the thickness of SiO_2 exponentially and then saturates. The saturation plateau is defined by other loss mechanisms. Therefore, the higher the quality of the fabrication is, the thicker layer of SiO_2 is required.

The radiative loss of BICs in periodic structures is suppressed due to the collective destructive interference from all the unit cells of the structure. Thus, quasi-BIC in the experimental samples have radiative losses that depend on the number of periods N (unit cells).^{67,125–128} The asymptotic behaviour of such losses (Q_{size}) for large N can be estimated from the known dependence of radiative losses in the infinite structure on the Bloch wavenumber, i.e. $Q_{\text{rad}} = Q_{\text{rad}}(\mathbf{k}_b)$. The transition from the infinite structure, which can be easily analyzed numerically or even analytically, to a finite one is based on the Fabry-Perot quantization of Bloch wavenumber. Thus, for the in- Γ BIC, Q_{size} is approximately $Q_{\text{rad}}(|\mathbf{k}_{b,\text{min}}|)$, where $|\mathbf{k}_{b,\text{min}}| \approx \pi/L$, and L is the linear size of the structure. Such an approximation has proven to be useful for linear chains.^{67,129} However, one should keep in mind that in some cases, the eigenmodes in an infinite lattice can substantially differ from those in finite structures even if their size is large.¹³⁰ In practice, the width of the high-Q Fano resonances ceases to depend on the sample size if it is about several hundred of periods. However, recently a dielectric structure design was proposed that consists of 27×27 Si blocks hosting a quasi-BIC with experimentally measured $Q_{\text{tot}} = 18500$ in the telecommunication range.¹¹⁹ However, there is no clear recipe how to fabricate high-Q metasurfaces with a small footprint, and today it remains a highly relevant challenge. The total Q factor of BICs in periodic dielectric structures is about 10^3 - 10^4 in the visible and near-IR ranges,^{49,67,92,120,129,131,132} and it

strongly depends on the fabrication quality. The radiative Q factor can reach values of 10^6 - 10^7 .⁴⁹ Recently, a symmetry-protected BIC in a photonic crystal slab with total Q factor of about 10^6 was demonstrated experimentally.¹³³ The radiation from the edges of the structure was suppressed by surrounding the sample with a photonic crystal with another lattice constant. Thus, the frequency of BIC was in the bandgap of the surrounding photonic crystal.

Another source of radiative losses is the radiation induced by fabrication imperfections or structural disorder. Such losses are a common problem for high-Q photonic structures.^{134–136} Structural fluctuations are much more difficult to control than, for example, the sample size. Therefore, the radiation losses due to structural fluctuation and fabrication imperfections usually are the main loss mechanism limiting the Q factor of BIC. It is well-known that the structural disorder in periodic photonic structures drastically affects their optical properties, resulting in non-trivial Fano resonance evolution, light localization, coherent back-scattering, etc.^{137–141} The disorder effects are most essential in self-assembled and natural photonic structures.^{142–144}

According to the general theory, the Q factor of BIC due to the structural fluctuations behaves as $Q_{\text{str}}^{-1} \propto \sigma^2$, where σ is the disorder amplitude.¹⁴⁵ In Ref.,¹⁴⁶ the Authors analyzed the radiative losses of symmetry-protected BICs in dielectric gratings using the coupled-mode theory, finite element methods and the supercell approach. They mention that the radiation is mainly induced by fractional-order Bloch waves, particularly near the zeroth order diffraction channel. Thus, we can say that fluctuations result in BIC scattering to the neighboring states (in k-space) states that are leaky. The Authors show that when the size of the unit cell becomes large enough, the influence of the boundary conditions becomes considerably weak. This can be explained by the spatial localization of the mode, but the Authors didn't analyze this effect. The spatial localization of the BICs was demonstrated numerically in Ref.,¹⁴⁷ where one-dimensional periodic structure composed of two layers of dielectric rods was considered. In the same work, the effect of the uncorrelated structural disorder was analyzed for both the symmetry-protected and accidental BICs. It was shown that the symmetry-protected BICs are more resistant to the fluctuation of the rods in the direction perpendicular to layers compared to the fluctuation of the rod position along the layers. And vice

versa, the accidental BICs are more robust against the fluctuation along the direction of periodicity. The Anderson localization effect in structures with BICs is discussed in Ref.¹⁴⁸ In this work, the Authors considered the structure similar to that considered by Plotnik et al. [see Fig. 2(c)]³¹ and analyzed in detail the stability of the BIC against disorder. They showed that due to the non-trivial interplay between the BIC and disorder-induced localized states, the entangled biphoton survives after averaging over all the disorder configurations.

The Authors of Ref.⁴⁸ proposed the idea how to increase the resistance of BICs to structural disorder. They experimentally demonstrated a BIC with the total Q factor about 5×10^5 . The main idea is to merge several BICs in the k-space in the vicinity of the Γ -point. Later, merged BICs, or super-BICs, in photonic crystal slabs were used to achieve record-low threshold lasing.¹²⁰ As we mentioned above, the radiation of BIC due to structural disorder occurs via the fractional-order Bloch waves near the Γ -point. Thus, in the proposed design, the rescattering takes place mainly between the extremely high-Q states, making the BIC immune against the structural disorder.

BICs in photonic structures of various dimensions

Gratings

In this section, we overview the BICs in 1D dielectric gratings – photonic structures of finite thickness periodic in one direction and having a translational symmetry in other direction. The study of such structures has a long history, which began in 1887 from Lord Rayleigh’s works.¹⁴⁹ The waveguide gratings were intensively studied since the middle of the 20-th century, and they found numerous applications in distributed-feedback lasers, laser mirrors, bandpass filters, wavelength demultiplexers, polarizers, chemical and bio-sensors, and other optic and optoelectronic devices. An interested reader may consult numerous reviews.^{150–154} A pronounced twist in the physics of optical gratings was related to the development of nanotechnology, namely, photonic crystals, metasurfaces, flat optics, and high-contrast gratings.¹⁵⁵

Due to simple geometry, the BICs in dielectric gratings can be described easily using the

Fourier modal method (FMM, also called rigorous coupled-wave analysis, RCWA)¹⁵⁶ or the true modal method (TMM)¹⁵⁷ designed to be particularly efficient for gratings, resonant state expansion,^{158,159} guided mode expansion,¹⁶⁰ multiple scattering theory (Korringa–Kohn–Rostoker method),¹⁶¹ and others. FMM and TMM methods supplemented with the S-matrix technique provide a powerful tool for analysis of complex multilayer and photonic crystal structures.^{53,162}

Along with the symmetry-protected BICs which we discussed previously, the gratings allow implementing another type of BICs, usually called *Fabry-Perot BIC*. It is well-known that in the vicinity of the optical resonances of non-absorbing gratings, the transmission becomes zero [see Fig. 4(b)],³⁹ i.e. the structure behaves as a perfect mirror. Using two such structures and varying the distance between them, one can completely trap the light between the gratings. This mechanism of BIC formation was analyzed in Ref.²¹ [see Fig. 2(a)]. The Fabry-Perot BIC is a particular case of tunable (Friedrich-Wintgen) BIC, and it also can be described within coupled-mode theory by Eqs. (1) and (2), assuming that $\omega_1 = \omega_2$ and $\gamma_1 = \gamma_2$. The Fabry-Perot BICs can appear at both normal $\mathbf{k}_b = 0$ and oblique $\mathbf{k}_b \neq 0$ incidence.

Actually, there is no need to use a double-layer structure to obtain a Fabry-Perot BIC. It can also appear in gratings with varying thickness. This is well-described by modal methods developed in Refs.^{163–167} In these approaches, Bloch modes are used that are propagating eigenmodes of the infinitely thick grating, similar to plane waves in free space.¹⁶³ A plane interface between a homogeneous medium and a photonic crystal couples the modes with each other (upon reflection) and with plane waves of the surrounding space or substrate (upon transmission), as illustrated in Fig. 13(a). As the slab is bounded by two interfaces, multiple Fabry-Perot-like resonances appear in the reflection spectra [see Fig. 13(b)]. One can see that the linewidth of the resonances strongly depends on the thickness of the grating t_g , and at particular values of t_g the resonances disappear from the spectra, turning into BICs. The appearance of the Fabry-Perot BICs requires the existence of two Bloch modes, at least, in the spectrum of the infinitely thick grating. Indeed, one can see from Fig. 13(b) that regardless of the slab thickness, BICs can exist only for $\lambda < \lambda_{c2}$. This condition defines the cutoff frequency of the second-order Bloch wave in the grating. This fact was

also used by Ovcharenko et al for the description of BICs in gratings.¹⁶⁸ They applied multimode Fabry-Perot model developed by Tishchenko¹⁶³ and Lalanne¹⁶⁴ and showed that the multimode Fabry-Perot model accurately predicts the existence of BICs and their positions in the parameter space. Using the same formalism, Bykov et al. obtained a simple closed-form expression predicting the BIC positions in the dispersion diagrams.¹⁶⁹ Similar results were obtained by Parriaux and Lyndin, but without any reference to BICs.¹⁷⁰

A further characterization of BICs in 1D gratings can be done in terms of S-matrix poles.^{53,171–173} The collapse of the Fano resonance for BICs means merging the zeros and poles of the S-matrix.¹⁷⁴ This condition can be used to find particular parameters at which the Fabry-Perot BIC appears.⁹⁷ Blanchard and co-authors¹⁷⁵ proposed a phenomenological approach based on pole-zero approximations of scattering matrix to describe the Fano resonances in the vicinity of BICs. Combining the pole and coupled-wave formalisms for waveguide resonances of a grating was done by Pietroy et al.¹⁷⁶ Authors⁴⁰ explained the ultra-narrow resonance corresponding to the accidental BIC via strong coupling between the guided modes. Using analytically known modes of planar waveguides as a basis, one can quantify describe the diversity of resonances of a photonic crystal slab via the resonant state expansion method,¹⁵⁹ which is also appropriate for BIC characterization.¹⁷⁷

Previously, we considered the gratings with up-down mirror symmetry. However, BICs can exist in gratings without such a symmetry. This problem was considered by Ndangali and Shabanov⁷² and Bulgakov et al.⁴⁷ Bulgakov and coauthors considered a grating consisting of a slab with ridges periodically arranged either on top or on both sides of the slab [see Ref. 14(a)]. In the case of two gratings, they are assumed to have the same period, but different permittivities, and they can be shifted with respect to each other by distance a . The Authors demonstrated that if a two-sided grating possesses either mirror symmetry with respect to the xy -plane or glide symmetry, i.e. a composition of a mirror reflection in the xy -plane and a half-period translation along the x axis, then the BIC are stable against variation of parameters as long as these symmetries are preserved. In this case, only a shift of the BIC along the dispersion curve occurs. If the up-down symmetry is broken due to the different geometries or material parameters of the lattices, the existence of

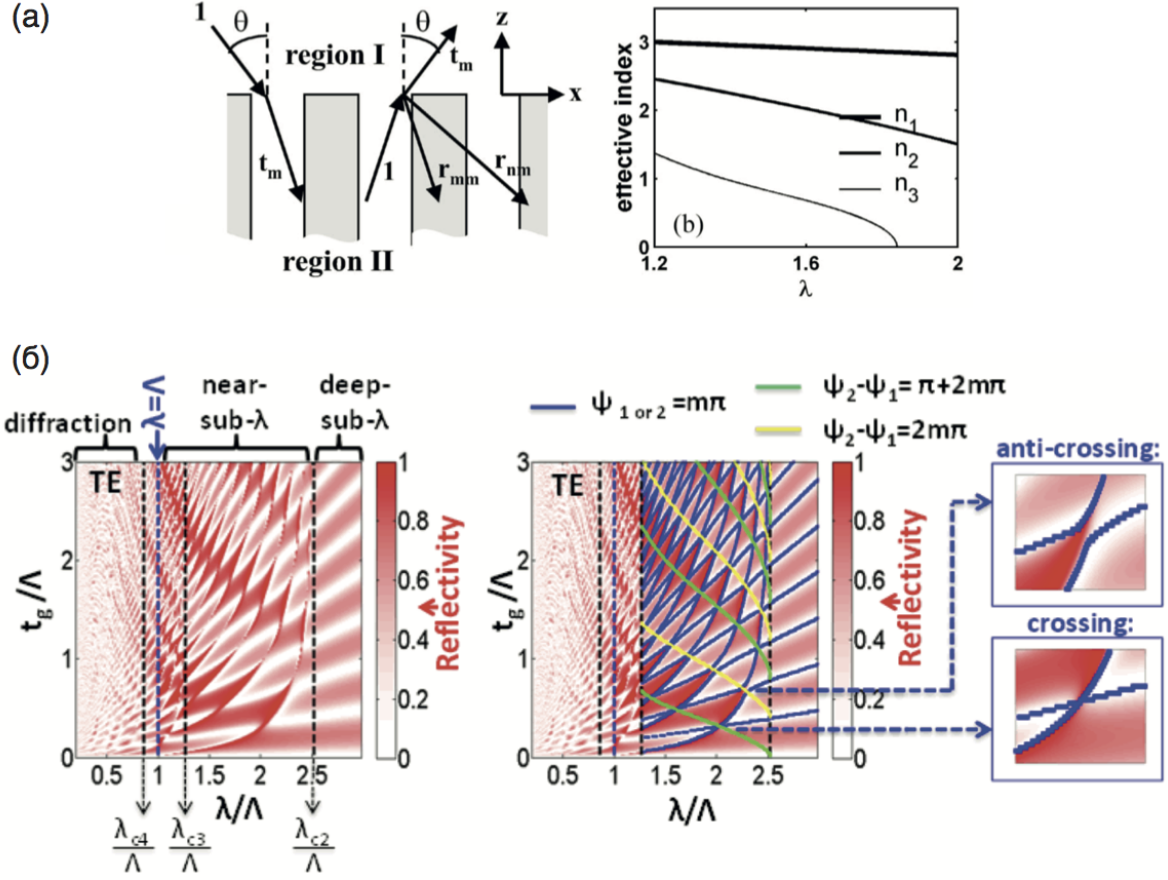


Figure 13: (a) Interface between a homogeneous medium and a semi-infinite 1D photonic crystal (left), and spectral dependence of effective propagation constants of Bloch modes in 1D photonic crystal (right). Adapted from Lalanne et al.¹⁶⁴ (b) Reflectivity maps for 1D photonic crystal slab: cut-off wavelengths of Bloch modes divide the map into areas with single-mode, two-mode, and multiple-mode regimes (left); blue lines identify the single-mode Fabry-Perot resonances, and green and yellow lines indicate the in-phase and anti-phase conditions in the two-mode regime (right). Adapted from Karagodsky et al.¹⁶⁷

the accidental off- Γ BIC requires a very fine adjustment of the system's parameters. Thus, such BICs are not robust against variation of the material or geometrical parameters of the structure. The obtained results are in complete accordance with those obtained earlier for by Ndangali and Shabanov, who considered double arrays of thin dielectric rods shifted with respect to each other⁷² shown in Fig. 14(b). They concluded that in the general case of an arbitrary shift of one lattice with respect to the other one results in the symmetry-protected BIC turning into the accidental BIC, and the accidental BIC turning into a high-Q quasi-BIC. In addition, the Authors show that BICs can exist, if two or three diffraction channels are open, but the existence of these BICs requires an

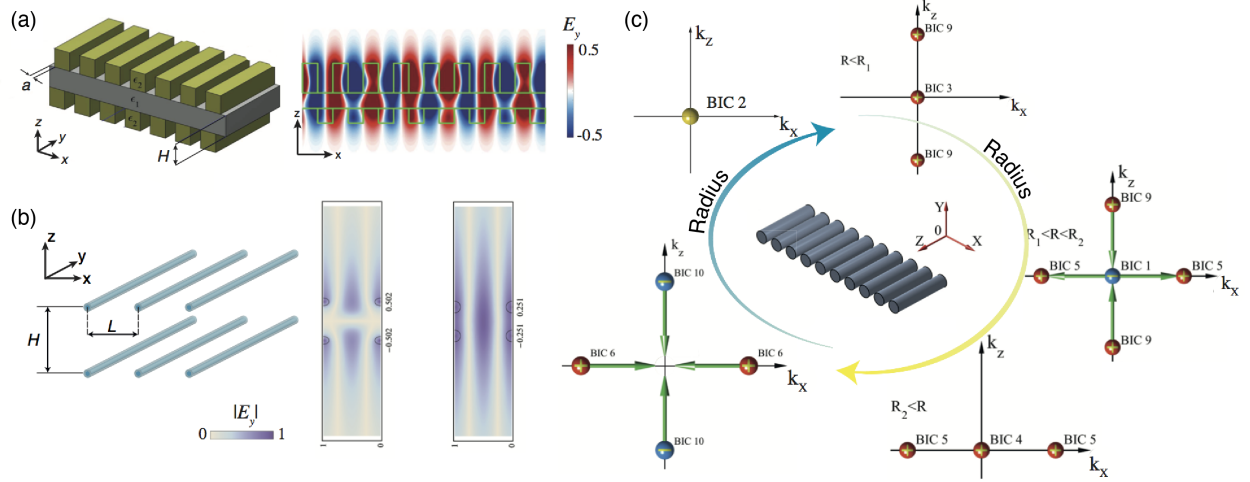


Figure 14: Bound states in the continuum in one-dimensional periodic structures. (a) Schematics of a double grating and E_y -field profile of the accidental off- Γ BIC. Parameter a is the shift in the xy plane, and H is the distance between layers. Adapted from Bulgakov E.N. et al.⁴⁷ (b) Schematics of a periodic structure composed of two arrays of dielectric rods, and the E_y -field profile of the accidental in- Γ BICs. Adapted from Ndangali et al.⁷² (c) Topological charges migration in a grating composed of dielectric rods. Yellow and blue arrows depict two different eigenmodes. Adapted from Bulgakov E.N. et al.¹⁷⁸

adjustment of the radius and permittivity of the rods.

Ndangali and Shabanov⁷² considered the BICs in an array of very thin rods, where each rod can be described within the Rayleigh approximation, i.e. $\sqrt{\varepsilon}k_0R \ll 1$, where k_0 is the wavevector in vacuum, R is the radius of the rods, and ε is their permittivity. Bulgakov and Sadreev generalized the considered problem to the case of arbitrary radius R and permittivity ε , using the multiple scattering theory in the T-matrix formalism.^{179–181} They considered an array of GaAs rods with $\varepsilon = 12$. The size parameter $\sqrt{\varepsilon}k_0R$ was in the range from 1 to 10. They showed that such a system supports three types of BIC: (i) symmetry-protected BICs with a zero Bloch vector, (ii) BICs embedded in one diffraction channel with nonzero Bloch vector, (iii) and BICs embedded in two and three diffraction channels. The first and second BIC types exist for a wide range of material parameters of the rods, while the third one occurs only at a specific value of the rods' radius or permittivity. Yuan and Lu considered a similar system numerically and determined the domains of the existence of BICs in the parametric space (R, ε) .¹⁸² Bulgakov and Maksimov studied finite arrays consisting of N parallel dielectric rods and analyzed the dependence of quasi-BICs and

resonances below the continuum (guided-mode resonances) on N .¹²⁵ They identified two types of BICs with radiative Q factors scaled as $Q \sim N^2$ and $Q \sim N^3$.

As we discussed previously, BICs in periodic structures can be considered as a polarization vortex with a certain topological charge, and this vortex can demonstrate non-trivial dynamics in k -space with the variation of the system's parameters, including annihilation, merging, and decay. All these effects were demonstrated in the Ref.¹⁷⁸ using the example of BICs in a periodic array of rods. Figure 14(c) shows the evolution of topological charges for two families of BICs.¹⁷⁸ Following the yellow arrow corresponding to the increase of the radius of the rods, one can see that the symmetry-protected (BIC 3) with $q = +1$ decays into two accidental BICs (BIC 5) with $q = +1$ and one symmetry-protected BIC (BIC 1) with $q = -1$. Further increase of the radius results in merging of two accidental BICs (BIC 9) in the Γ -point with the symmetry-protected BIC (BIC 1). It is worth mentioning that due to $\omega(-\mathbf{k}) = \omega(\mathbf{k})$ symmetry, off- Γ BICs emerge and disappear in pairs. Annihilation of topological charges in the Γ point may lead to the creation of both accidental and symmetry-protected BICs. The type of the forming BIC is defined by the total topological charge conservation law. Figure 14(c) (evolution along the blue arrow) illustrates the creation of the accidental in- Γ BIC $q = 0$ when two BICs labelled as BIC 6 with $q = +1$ merge with two BICs labelled as BIC 10 with $q = -1$.

The value of topological charge determines the asymptotic dependence of the radiative Q factor on the Bloch wavenumber. Due to the C_2 symmetry, one-dimensional periodic structures possess BICs with topological charges $q = 0$ or $q = \pm 1$.⁴⁶ The Q factor of an isolated BIC with $|q| = 1$ scales as $Q \sim 1/(k \pm k_{\text{BIC}})^2$.^{48,178,183} For example, the Q factor of the symmetry-protected BIC decreases as k^{-2} . Approaching the point of the annihilation, the dependence changes to $Q \sim 1/(k - k_{\text{BIC}})^2(k + k_{\text{BIC}})^2$ for both accidental in- Γ and symmetry-protected BICs. The inverse fourth-power relation indicates that the quality factor can be very large, even when $|k - k_{\text{BIC}}|$ is not small.¹⁸³ However, if the system parameters are detuned from this regime, the Q factor of the symmetry-protected BICs decreases as $Q \sim 1/k^2$ again. These asymptotic dependencies are extremely important, as they determine the radiative losses of quasi-BICs in finite-size structures

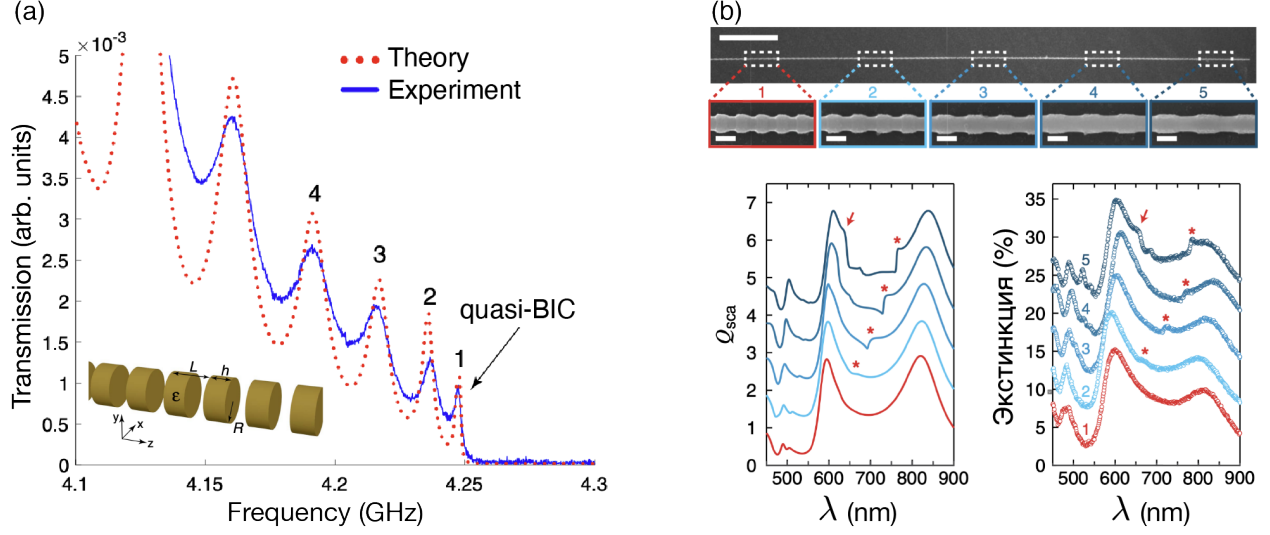


Figure 15: (a) Experimental transmission spectra of a chain consisting of 20 ceramic disks placed between two coaxially positioned loop antennas shown in the inset. The dotted line shows the results of numerical simulations carried out in COMSOL MULTIPHYSICS. The last peak in the series corresponds to quasi-BIC. Adapted from Sadrieva et al.⁶⁷ (b) Upper: SEM image of a nanowire containing five superlattices sections; the scale bar is 10 μm . Bottom: simulated scattering efficiency spectra (left) and experimental extinction spectra (right) (spectra offset by 5%) of the geometric superlattices. Adapted from Kim et al.¹⁸⁴

and their robustness to disorder.^{48,67,129}

1D periodicity with axial symmetry

1D periodic structures with axial symmetry [corrugated cylindrical waveguides, and chains of spheres or disks (see the inset in Fig. 15(a))] can also support different types of BICs. The theory of BICs in such structures was formulated by Bulgakov and Sadreev¹²⁸ and further developed in Refs.^{69,96,99} Owing to the axial symmetry and periodicity of the structure along the z -direction, the solution can be written in the following form

$$\mathbf{E}(r, \varphi, z, t) = \mathbf{u}_{m,k_z}(r, z)e^{-i\omega t \pm ik_z z \pm im\varphi}, \quad (20)$$

where φ is an azimuthal angle, m is the azimuthal quantum number, k_z is the Bloch wavenumber, and \mathbf{u}_{m,k_z} is a periodic function of z . In the special case of $m = 0$, the solutions of Maxwell's

equations in cylindrical coordinates can always be divided into TE and TM polarizations.¹⁸⁵ It is worth mentioning that in contrast to uncorrugated waveguides, in our case, the solutions do not split into two independent polarizations for $k_z = 0$, as k_z is the quasi-wavenumber which is determined up to the reciprocal lattice vector. Thus, for $k_z = 0$ and $m \neq 0$, all the modes have hybrid TE-TM polarization, as well as for $m = 0$ and $k_z \neq 0$. Therefore, the modes with $k_z = 0$ and $m = 0$ have only one open diffraction channel in subwavelength structures. For the odd modes with respect to the reflection in the xy plane, see Fig. 15(a), the coupling to this diffraction channel can vanish because of symmetry reasons, similar to the case of dielectric gratings. Therefore, subwavelength structures with a symmetric potential ($\varepsilon(-z) = \varepsilon(z)$) support the symmetry-protected BICs in the Γ -point. For the modes with $m \neq 0$ at the Γ -point, the radiative losses to one channel (TE or TM) can vanish due to the symmetry of the mode. The losses to the second channel can be nullified by fine adjustment of the system's parameters. Bulgakov and Sadreev named such states partially symmetry-protected BICs in the work.¹⁸⁶ They also demonstrated that BICs with $m \neq 0$ and $k_z \neq 0$ can be created by fine tuning of the chain parameters. As we mentioned previously, BICs in the periodic chain can be characterized by the topological charge, similar to BICs in 2D periodic structures. However, it is still unclear how to measure this charge experimentally.

BICs in a periodic chain were observed experimentally for the first time in the GHz frequency range, in an 1D array of coupled ceramic disks [see Fig. 15(a)].⁶⁷ To observe the symmetry-protected BIC, two identical loop antennas were used as magnetic dipoles: they were placed coaxially with the chain and connected to ports of a vector network analyzer. The measured and calculated transmission spectra are shown in Fig. 15(a). The last peak in the series corresponds to a quasi-BIC, which turns into a genuine BIC in the infinite chain. It was shown that the total Q factor of the quasi-BIC grows quadratically with the increase of the number of periods and then saturates at the level $Q = 4000$ due to the material absorption. An accidental BIC ($m = 0, k_b = 0$) was observed experimentally in a similar system in Ref.¹²⁹ The linear growth of Q factor with the number of disks was demonstrated for the observed accidental off- Γ BIC. On the contrary, the radiative Q factor of the accidental in- Γ BIC follows the scaling law as $Q \sim N^3$ with N being the

number of scatterers in the array.¹²⁵

The first experimental observation of a BIC in an axially symmetric periodic structure in the optical range was presented in 2019.¹⁸⁴ The Authors fabricated a silicon nanowire with a periodic grating at the surface as shown in Fig. 15(b). The surface grating forms a structure similar to a periodic array of disks placed coaxially on a core. Since the nanowire was illuminated by a plane wave at normal incidence, quasi-BICs with different m were excited. The Authors analyzed both theoretically and experimentally how the appearance of a BIC depends on illumination and geometry of cylindrical nanowire. The BIC-induced light confinement in such structures can be used to substantially enhance absorption, which can be applied in photodetector or photovoltaic devices incorporating a p-i-n diode design and based on nanowires with superlattices.¹⁸⁷

Nanowires with a periodic superlattice, and arrays of disks have advantages over the array of spheres due to a larger number of degrees of freedom. By independent adjustment of the period, height, and radius of the disks, one can provide precise mode engineering, and obtain several BICs with different orbital angular momenta and Bloch vectors. Such linear chains supporting BICs can be used as a compact source of optical beams with angular momentum.

2D periodicity. Photonic crystal slabs

In this section, we review the main properties of BICs in photonic crystal slabs (waveguides) - 2D dielectric photonic structures that have a band gap for the waves propagating in the waveguide plane and that use index guiding to confine light in the third dimension. Since 1990s, such structures are considered easier for fabrication than photonic crystals with full three-dimensional band gaps, while retaining many of the latter's desirable properties.^{188,189} Compared to 1D structures, photonic crystal slabs provide a broader variety of designs for unit cells, different types of their arrangement and, consequently, more degrees of freedom for flexible control over their optical properties.^{160,190} Due to this fact, the variety of BICs in such structures is more extensive than for one-dimensional gratings or chains, including the possibility of BICs with high-order (≥ 2) topological charges⁴⁶ and robustness to disorder.⁴⁸

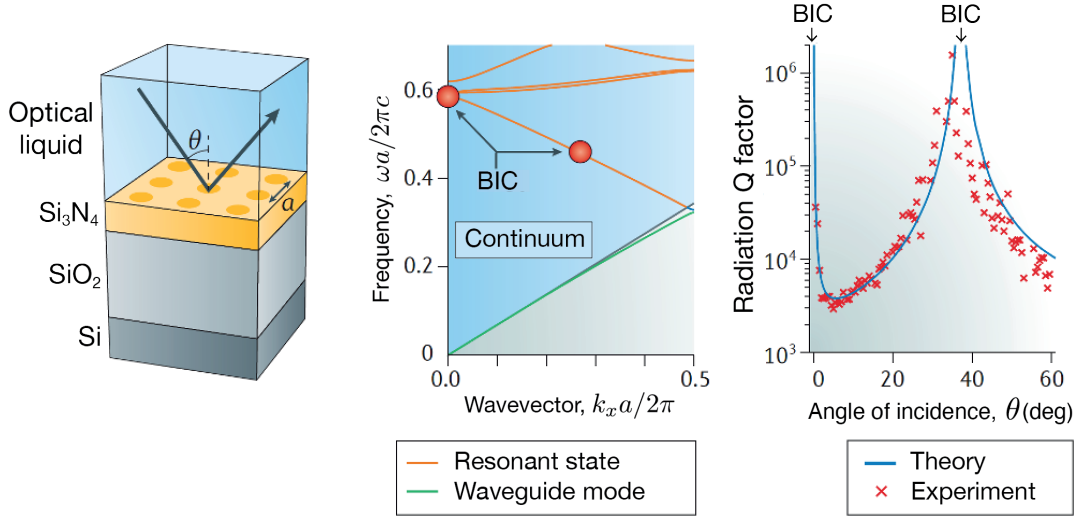


Figure 16: Left: schematic layout of the fabricated structure, immersed in a liquid, index-matched to silica at 740 nm. Center: The band structure along Γ -X direction with TM polarization. The BICs are marked with red dots. Right: normalized radiative lifetime extracted from the experimentally measured reflectivity spectrum (red crosses). The blue solid line shows the prediction from FDTD. Adapted from Hsu et al.⁴⁹

The first systematic study of BICs in photonic crystal slabs was performed in 2013⁴⁹ for a Si₃N₄ slab patterned with a periodic arrangement of circular holes as shown in Fig. 16, left panel. The slab was grown on a SiO₂/Si substrate and immersed in a liquid, index-matched to silica, which was important to keep the up-down reflection symmetry required for observation of accidental BICs. The band structure for TM-like modes along the Γ -X direction is shown in Fig. 16, central panel. The structure supports a symmetry-protected BIC at the normal incidence and an accidental BIC at a non-zero Bloch vector corresponding to an oblique angle of incidence around 35 degrees, as can be seen in Fig. 16, right panel. The red crosses show the values of the radiative Q factor calculated from the total Q factor, which was extracted from the measured reflectivity spectra by assuming the value of non-radiative Q factor equal to 10⁴. The achieved value of radiative Q factor for the accidental BIC reaches 10⁶; however, the value of the total Q factor remains limited to 10⁴ because of parasitic and non-radiative losses. This work was the first direct evidence of true accidental BICs measured experimentally, to the best of our knowledge.

The physics and origins of accidental BICs were analytically described in Ref.¹⁹¹ within a coupled-wave theory (CWT) developed specially for description of response for 2D photonic crys-

tal slabs.¹⁹² Within this approach, the electromagnetic fields of eigenmodes of a photonic system are expanded into guided modes and radiative modes of a uniform waveguide, which are used as basis functions. Due to the interaction with the lattice, the guided modes also have radiative losses. Thus, both the guided and leaky modes can contribute to the same radiation channels (diffraction channels) due to the interaction with the periodic potential of the structure. In the work,¹⁹¹ it was shown that accidental BICs are formed due to the destructive interference of all the basis functions: both the guided and leaky ones. Two reasons of destructive interference were indicated. First, the contributions from equivalent directions in the reciprocal space can result in spontaneous appearance of an additional symmetry and, thus, to the formation of an accidental BIC. An example of such a BIC is presented in the work.⁴⁹ Second, it was shown that accidental BICs do not necessarily occur exactly at a high-symmetry point in the reciprocal space. The reason is, in contrast to symmetry-protected BICs, for accidental BICs, the guided basis modes contribute to the open radiation channels of the photonic structure with different weights and, therefore, after the radiation is cancelled at the symmetry point, some residual radiation can still remain. In other words, the point corresponding to a BIC in the reciprocal space does not always have a high symmetry, but is located near such a point. This is typical for the Friedrich-Wintgen mechanism.^{7,193} Furthermore, it was shown analytically that the locations of accidental BICs can be shifted by changing various parameters, such as the cladding permittivity or geometrical sizes of the waveguide. It is worth mentioning that in other works, analytical considerations demonstrate that the energy of symmetry-protected BICs is confined dominantly in the closed diffraction channels of the \pm orders.

The moderate value of the total Q factor of 10^4 in Ref.⁴⁹ is related to the out-of-plane losses originating in realistic samples due to finite size of samples and fabrication imperfections. Recently, a new approach was suggested, which allows suppressing the out-of-plane losses, using the topological nature of BICs, namely, by merging several BICs at the Γ point in the k-space.^{48,194} In the paper, the Authors considered a 2D dielectric photonic crystal membrane suspended in air. The fundamental TE-band of the membrane supported one symmetry-protected BIC at the Γ point and

eight accidental BICs located symmetrically around the Γ point. The tunability of accidental BICs allows moving them away from an off- Γ position towards the center of the Brillouin zone. The experimentally measured value of 5×10^5 was demonstrated for the total Q factor in the merging regime. For a single isolated BIC with a ± 1 charge, the Q factor of standard symmetry-protected BICs decays quadratically ($Q \sim 1/k^2$) with respect to the distance k from the Γ point. However, it was shown that the scaling changes to $Q \sim 1/k^6$ in the configuration in which all nine BICs merge. Later, it was shown that for finite-size samples, the highest Q factor can be achieved not for the complete merging condition, but in the pre-merging regime, when the accidental BICs lie on the circle of a small radius in the k-space.¹²⁰

One of the remarkable properties of 2D periodic photonic structures is that a BIC can exist even in chiral samples without the in-plane inversion symmetry.¹⁹⁵ In general, a BIC in the sub-diffractive regime can be achieved via cancellation of radiation into both polarization channels. In Ref.,¹⁹⁵ the Authors showed that by using a cross-shaped periodic photonic structure without a second-order symmetry axis, it is possible to cancel radiation amplitudes for both polarizations: one polarization channel is suppressed due to the vertical mirror plane, and another one parametrically, tuning the geometry of the unit cell. This mechanism of BIC formation is very similar to the one considered by Bulgakov and Sadreev for obtaining partially symmetry-protected BICs in a chain of dielectric spheres.¹⁸⁶

Individual subwavelength resonators

For individual subwavelength resonators, genuine nonradiative states require extreme values of permittivity, tending toward infinity or zero^{62,198,199} or imitating periodic boundary conditions with metallic waveguides.^{65,200,201} In realistic individual resonators, there is always an infinite number of radiation channels, which limits the Q factor substantially. However, the concept of quasi-BICs allows reaching almost nonradiative states for individual dielectric resonators. Using the parameter-tuning approach originally developed by Friedrich and Wintgen⁷ and later used for some extended geometries,²⁰² one can create high-Q quasi-BICs in compact geometries at subwavelength scales.

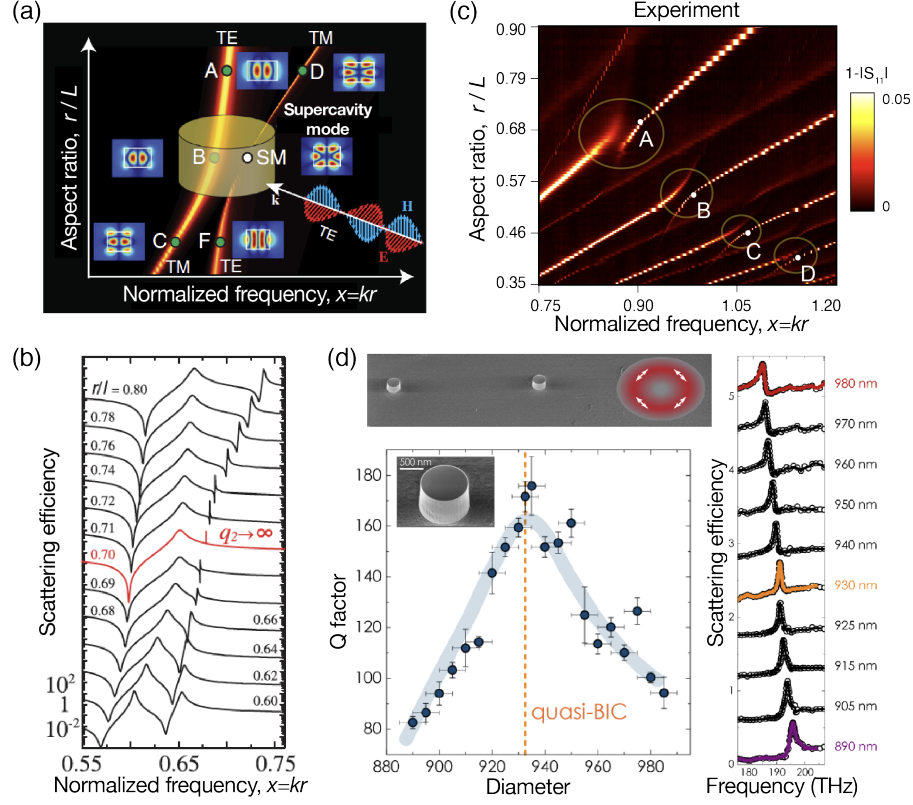


Figure 17: (a) Illustration of strong mode coupling and a bound state in the continuum supported by a high-index dielectric resonator. (b) Simulated scattering spectra of a nanodisk with $\varepsilon = 80$ and azimuthal quantum number $m = 0$. Adapted from Rybin et al.¹⁹³ (c) Measured map of the coefficient $1 - |S_{11}|$ versus frequency kr and aspect ratio r/L for a ceramic nanodisk with $\varepsilon = 44.8$. The quasi-BICs labeled as A–D correspond to aspect ratios $r/L = 0.71, 0.55, 0.47$, and 0.42 , respectively. Adapted from Odit et al.¹⁹⁶ (d) Upper: SEM image of several isolated nanodisks and electric field distribution for an azimuthally polarized incident wave. Lower: dependence of the experimental-extracted Q factor of a quasi-BIC on the disk diameter. Right: measured reflectance spectra of nanodisks with different diameters. Adapted from Melik-Gaykazyan et al.¹⁹⁷

In a very recent work,²⁰³ implementation of quasi-BICs, called there supercavity modes, was proposed in individual dielectric resonators via continuous tuning of the resonator's aspect ratio. Such parameter tuning enables destructive interference and strong coupling of two leaky modes (radial and axial) when their frequencies come close. Importantly, the modes forming a quasi-BIC belong to the same resonator should have the same symmetry.

The concept of the mentioned supercavity mode is shown in Fig. 17(a). The map demonstrates the contribution of the modes with zero azimuthal index to the scattering cross section of a high-index dielectric disk with respect to dimensionless frequency and disk aspect ratio. The

radial and axial modes interact strongly in the vicinity of the avoided resonance crossing, which results in sharp narrowing of the linewidth for one of the modes - supercavity mode. The second mode demonstrates a broadening of the linewidth according to the general properties of open non-Hermitian systems⁵⁸ [see also Fig. 6(b)]. The proposed hybrid mode profiles are a combination of radial and axial oscillations in the vertical cross-section and a uniform azimuthally symmetric distribution in the horizontal cross-section. The formation of quasi-BICs can be identified by the special features of the lineshape in scattering spectrum. For a high-index disk with a permittivity of 80, the lineshape changes from an asymmetric Fano profile to a symmetric Lorentzian in the vicinity of supercavity mode formation, as shown in Fig. 17(b). This change corresponds to diverging Fano asymmetry parameter q . Such behaviour was later explained within the framework of interference of different modes with very similar far-field profiles.^{204,205} In the case in Fig. 17(a), both interacting modes are dominated by magnetic dipolar contribution. The dipole contributions can cancel each other via mode interference, which makes the next allowed multipole (in this case, magnetic octupole) contribution dominant. The formation of quasi-BICs with nonzero azimuthal indices is also possible, but it leads to lower Q factors due to lower symmetry of the field profile.

The first experimental observation of quasi-BICs was carried out quite recently in microwave¹⁹⁶ and near-IR^{197,206} ranges. Figure 17(b) shows the measured spectral map of the reflection coefficient $1 - |S_{11}|$ for a single ceramic disk with permittivity of 44.8 from Ref.¹⁹⁶ The excitation was performed in the near field with a loop antenna, which selectively excites the modes with zero azimuthal index. The spectra reveal four avoided resonance crossings corresponding to formation of quasi-BICs. The radiative Q factor of quasi-BICs reaches 200000, but due to the absorption in the ceramic material, the maximal measured unloaded total Q factor is 12500. The observation of supercavity modes in near-IR was carried out for isolated AlGaAs nanodisks on engineered three-layer substrate with a reflective layer of ITO in the middle.^{197,206} The SEM image of individual nanodisks is shown in the upper panel of Fig. 17(c). The measured spectra and extracted Q factor for a range of the disk diameters is shown in the lower panel of Fig. 17(c). The maximum measured Q factor is approximately 180 for a disk with 930 nm diameter. The spectra reveal that the

lineshape is Fano-like and changes its asymmetry in the vicinity of the quasi-BIC, as was predicted theoretically for a single disk in vacuum. To match the mode symmetry and excitation, a tightly focused azimuthally polarized Gaussian beam was used.

Later, several generalizations were suggested for quasi-BICs in non-periodic finite resonators. For example, two coaxial disks were suggested as a structure supporting quasi-BICs with much higher values of Q factor than that of a single disk.²⁰⁷ Additionally, Bragg reflectors were suggested to further increase the Q factor of an individual quasi-BIC disk.²⁰⁸ The multipolar classification of eigenmodes in single resonators of different shapes was suggested later, based on the symmetry group theory.²⁰⁹ These results lead to prediction of quasi-BICs in dielectric spheroids,²¹⁰ triangular prisms,²⁰⁹ bar-shaped microcavities²¹¹ and resonators of arbitrary shapes.²¹²

Asymmetric metasurfaces and quasi-BICs

Recently, it was demonstrated that broken-symmetry dielectric metasurfaces demonstrate sharp peaks in the normal incidence transmission spectra, which are associated with quasi-BICs excitation.¹¹⁰ It was shown that the in-plane asymmetry induces an imbalance of the interference between counter-propagating leaky waves, resulting in the formation of a quasi-BIC. This effect was observed in a variety of metasurfaces in different frequency ranges and was connected to electromagnetic field-induced transparency,²¹³ tunable high-Q resonances,²¹⁴ trapped-mode resonances,²¹⁵ broken-symmetry Fano metasurfaces^{216,217} and dark modes.²¹⁸

Figure 18(a) shows the scattering of light by an asymmetric metasurface. The radiative Q factor of quasi-BICs in asymmetric metasurfaces follows the typical inverse quadratic dependence on the meta-atom asymmetry parameter α ,¹¹⁰ as shown in Fig. 18(b), left panel. In the regime of transmission (or reflection), the quasi-BICs manifest themselves as sharp asymmetric Fano resonances whose width and depth decreases with the decrease of α , as shown in Fig. 18(b), right panel. The total Q factor of the quasi-BIC mode is limited by other losses (see Section 'Losses and Q factor of quasi-BICs'). Due to parasitic effect of other losses, the maximal field enhancement can be

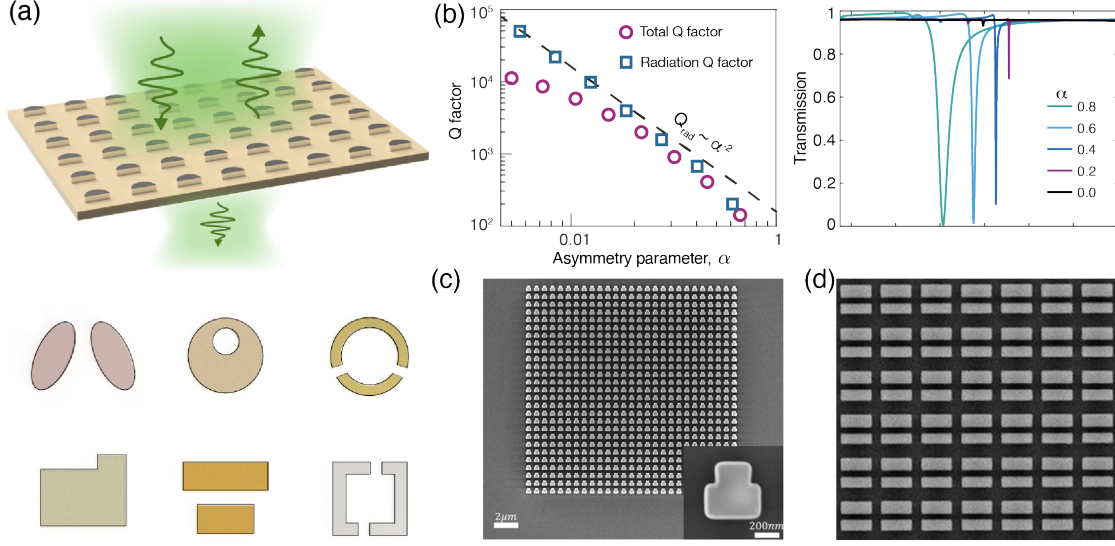


Figure 18: (a) Schematic for the scattering of light by a metasurface, and designs of the unit cells of asymmetric metasurfaces with a broken in-plane inversion symmetry of constituting meta-atoms supporting sharp resonances. (b) Typical dependence of the total (circles) and radiative (squares) Q factor of the quasi-BIC on the meta-atom asymmetry parameter α and characteristic evolution of the transmission spectra by changing α . (c,d) SEM images of silicon metasurfaces used in recent experimental demonstrations of quasi-BICs with a very high Q factor of approximately 18500 (c) and 750 (d). Adapted from Koshelev et al.^{110,206}

achieved not for minimal radiative losses, but in the regime of optimal (critical) coupling when the rates of radiative and parasitic losses are equal, $Q_{\text{abs}} = Q_{\text{rad}}$.^{114,115} Very recently, quasi-BICs with giant values of the Q factor in Si metasurfaces were experimentally demonstrated for different designs of meta-atoms. Figures 18(c) and 18(d) show the SEM images of two metasurfaces hosting the quasi-BICs with a Q factor of about 18500,¹¹⁹ and 750,²¹⁹ achieved by smart engineering of radiative losses and advanced electron-beam lithography techniques. Later, it was shown that even a true BIC can exist in an asymmetric metasurface in specific conditions.¹⁹⁵ Metasurfaces with strong asymmetry were used to create near-unity chiral response.^{220–222}

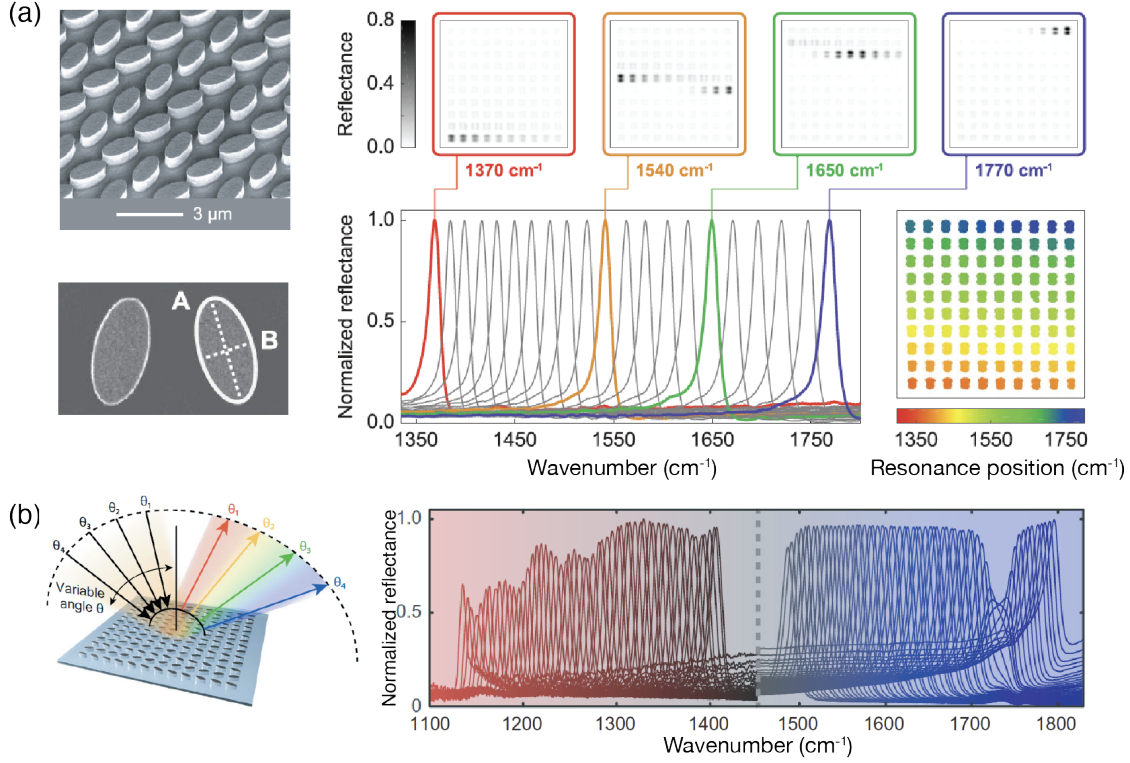


Figure 19: (a) SEM image of a metasurface and its meta-atom. Reflection images of a pixel metasurface obtained for four given wavelengths in the mid-IR range. Normalized reflection spectra for 21 out of 100 metapixels. Based on A. Tittl et al.²²³ (b) A germanium-based dielectric metasurface supporting quasi-BIC with angle multiplexing. Reflection spectra after deposition of a thin film of polymethyl methacrylate with centrifugation. Based on the work of A. Leitis and colleagues²²⁴.

BIC applications: optical detection, laser generation, nonlinear optics

BICs and quasi-BICs are widely used for various applications in photonic crystal slabs, waveguides, single subwavelength particles and other platforms. BIC-based applications include filtering,^{225–228} lasing,^{71,92,100,120,229–235} magnetophotonics,^{236–239} detection of biological objects,^{219,223,224,240–248} nonlinear generation and self-action,^{22,29,115,121,122,183,249–260} vortex generation,^{94,102,261} on-chip photonic devices,^{97,228,262–264} switches driven by external voltage,²⁶⁵ active THz devices,²⁶⁶ optical tuning of halcogenide metasurfaces,²⁶⁷ enhancement of chiral nonlinear response,²⁶⁸ polaritonics,^{269–275} and harmonic generation in hybrid structures with monolayers of transition metal dichalcogenides.^{276,277} Moreover, BICs in single nanoparticles were used to achieve a record-high ef-

efficiency of second-harmonic and higher harmonic generation,^{206,278–280} generation of quantum-entangled photons,²⁸¹ and low-threshold lasing.⁸⁸

We will consider several applications in more detail. Passive photonic structures supporting BICs recently were used to increase the efficiency of biological objects' detection. In the work,²²³ Tittl et al. implemented a nanophotonic sensor of biomolecules in the mid-IR range, based on the reflection from a dielectric matrix of metasurfaces supporting BICs. In Fig. 19(a), the left panel shows SEM images of an asymmetric silicon metasurface and its meta-atoms. The proposed structure supports quasi-BICs in the mid-IR range with a Q factor of approximately 200. The right panel shows reflection images of a pixel metasurface obtained for four given wavelengths and normalized reflection spectra for 21 out of 100 metapixels. Due to the narrow quasi-BIC resonance in the reflection spectrum and its tunability with changes in the geometric dimensions of the metasurface, a method based on this structure for distinguishing the absorption spectra of various molecules was demonstrated. In the work²²⁴ by Leitis et al., an asymmetric silicon metasurface with BICs was used for angle multiplexing of spectra, which also allowed a convenient distinguishing of absorption spectra of various biomolecules. Figure 19(b) shows a metasurface multiplexing scheme and reflection spectra from the structure. In another series of works by Romano et al.,^{131,244,282} the sensitivity of sensors based on photonic crystal waveguides with BICs was studied to changes in the refractive index of the external medium, and high sensitivity was experimentally shown to be achieved due to BICs. In a recent work by Jahani et al.,²⁴⁸ BIC-based silicon metasurfaces with a complex unit cell were developed for the detection of extracellular vesicles of cancer cells.

Photonic structures with BICs are widely used in active photonics, including for laser generation. Figure 20(a) shows the output power spectra depending on the wavelength and pump power for a 16×16 metasurface supporting BICs in the near-IR range from.⁷¹ In this work, the Authors used a tunable accidental BIC with a wavelength of 1550 nm. The right panel of Fig. 20(a) shows the dependence of the output power on the pump power at resonance. As the pump power is increased to 60 μ W, a distinct peak is observed in the emitted power spectra at the BIC wavelength. The inset shows a SEM image of the structure. In a recent paper,¹²⁰ lasing from the so-called

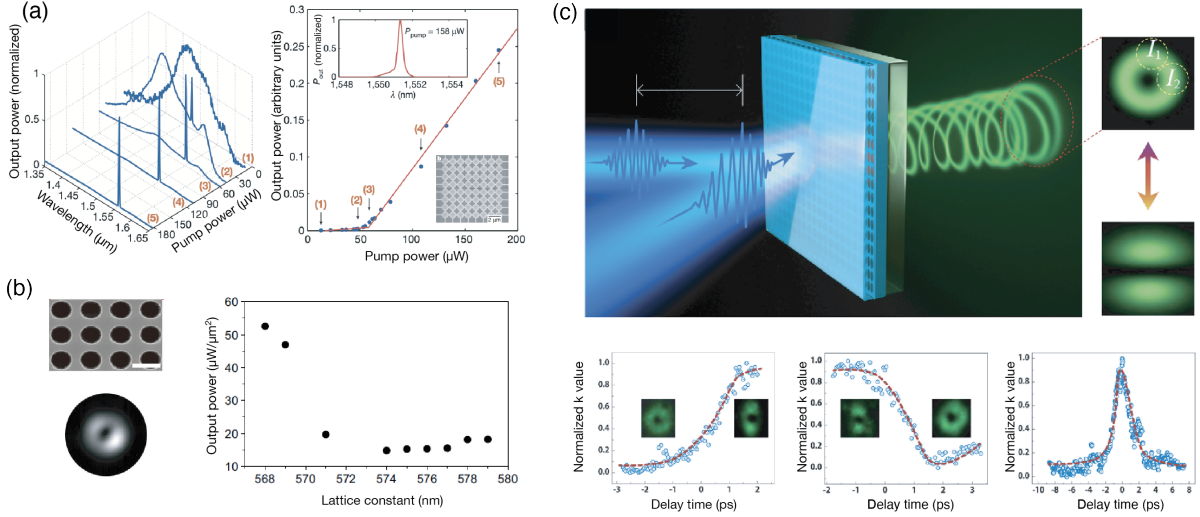


Figure 20: (a) Change in the normalized output power as a function of wavelength and pump power for a metasurface. Output power as a function of the average pump power (light curve) at the lasing wavelength. An image of the 16×16 metasurface is shown in the inset. Based on Kodigala et al.⁷¹ (b) SEM image of a photonic crystal waveguide and measured far-field profile for a super-BIC laser. The value of the lasing threshold normalized to the pumping area ($5.4 \mu\text{m}$ in size) as a function of the lattice parameter. Based on M. Hwang et al.¹²⁰ (c) Top: Schematic of a two-beam pumping experiment. The insets show far-field radiation patterns of a perovskite photonic structure for symmetric and asymmetric pump beam profiles. Bottom: Evolution from vortex laser generation to linearly polarized generation and the reverse process. Transition from an annular beam to a two-lobe beam and back on the scale of several picoseconds. Based on the work of Huang et al.¹⁰⁰

super-BIC, i.e. several BICs combined in the momentum space and having the same frequency, was studied. A distinctive feature of a super-BIC is a higher stability of the mode against deviations from periodicity and imperfections in the surface of the structure. The left panel of Fig. 20(b) shows a SEM image of an InGaAsP photonic crystal waveguide and the measured far-field profile for a mode of the super-BIC laser. Laser generation in the structure is achieved through the use of quantum dots in the layer. As shown in Fig. 20(b), the spot in the Fourier space has a small angular divergence, which is a hallmark of strongly confined modes. The right panel of Fig. 20(b) shows the lasing threshold normalized to the pumping area ($5.4 \mu\text{m}$ in size) as a function of the lattice parameter of the structure. The super-BIC state is realized at a lattice parameter of about 573 nm : in this regime, the lasing threshold is the lowest and has a record low value among all BIC lasers and lasers based on topologically protected states.¹²⁰ In the work of Huang et al.,¹⁰⁰ vortex

microlasers were studied, based on perovskite photonic crystal waveguides supporting BICs in the visible range, for ultrafast optical switching at room temperature. The Authors have experimentally demonstrated switching between vortex beam generation and linearly polarized beam generation, with a characteristic switching time from 1 to 1.5 picoseconds and a record low power consumption. The top panel of Fig. 20(c) shows the scheme of the experiment on two-beam pumping of a perovskite photonic structure. The insets show far-field radiation patterns for symmetric and asymmetric pump beam profiles. The lower panel shows the transition from vortex laser generation to linearly polarized generation and the reverse process on the scale of several picoseconds. S. Ha et al.²³¹ studied a laser based on a gallium arsenide metasurface supporting a BIC at a wavelength of about 825 nm. Azzam et al.²³³ studied single-mode and multimode lasing in the visible range based on a similar titanium dioxide metasurface coated with a thin layer of an organic dye. In this work, it was experimentally shown that directed radiation can be achieved by adjusting the period of the metasurface due to the BIC properties. In a recent work by Yang et al.,²³⁵ lasing based on an asymmetric Si_3N_4 metasurface coated with a rhodamine 6G dye with strong fluorescent properties was studied. In this work, lasing at a wavelength of approximately 600 nm was experimentally demonstrated due to the excitation of a quasi-BIC. S.Dyakov et al.⁹² showed a significant increase in the photoluminescence from a silicon photonic-crystal waveguide with germanium nanoislands, which supports BICs in the near-IR range.

BICs and quasi-BICs are studied most actively in nonlinear optics and photonics applications, mainly in order to enhance nonlinear generation and to observe the self-action of an exciting pulse. In a series of works by K. Koshelev et al.,^{29,115} optical second- and third-harmonic generation was studied in nonlinear dielectric metasurfaces with asymmetric unit cell, supporting quasi-BICs with Q factor depending on the asymmetry. In particular, in the work,¹¹⁵ the fabricated metasurface had a low Q factor of approximately 160 due to the presence of strong surface roughness. In this work, it was shown theoretically and experimentally that for such non-perfect photonic structures, the highest efficiency of harmonic generation is achieved not at the highest Q factor, but in the critical coupling regime, when the radiative Q factor is equal to the Q factor related to all the other

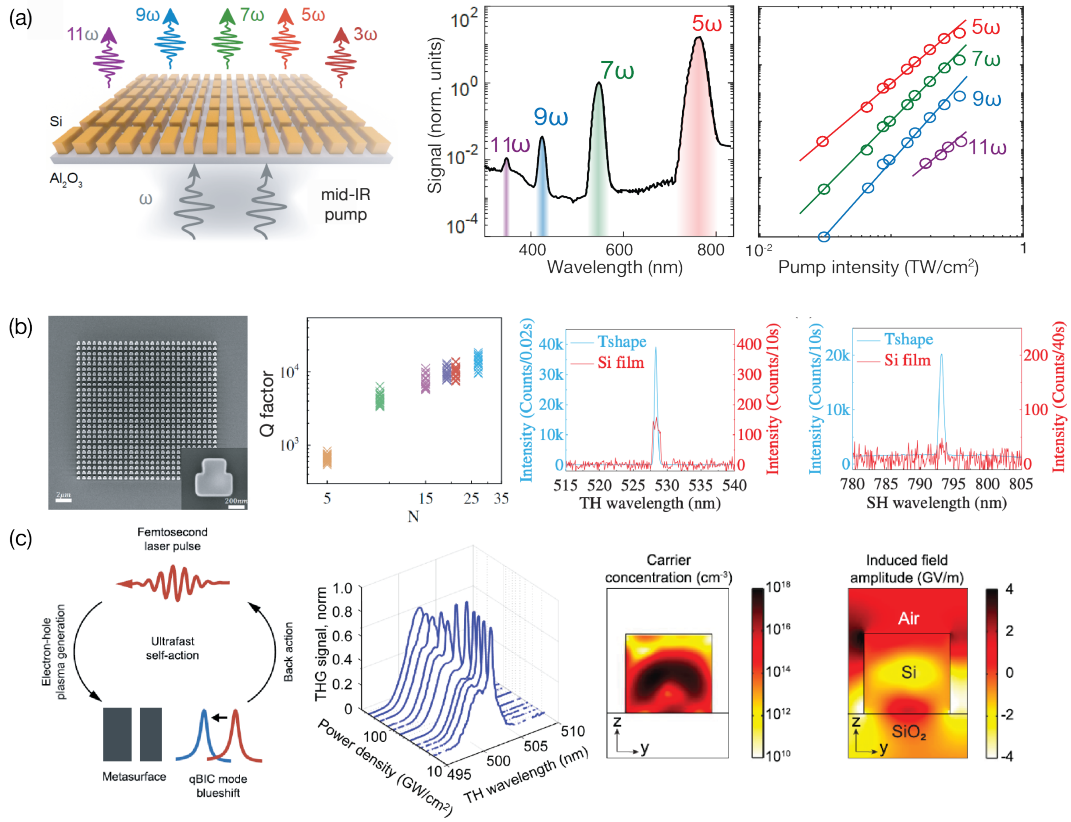


Figure 21: (a) The spectrum of the signal from the 3rd to 11th harmonics from an asymmetric silicon metasurface with BICs, and the dependence of the harmonics' power on the pump pulse power. Based on G. Zograf et al.²⁵⁹ (b) Statistics of the measured Q factors of the BICs for all the fabricated silicon metasurfaces with different sizes. The spectra of the second and third harmonics for a metasurface and an unstructured film. Based on J. Liu et al.¹¹⁹ (c) Scheme of ultrafast self-action of a pulse through a BIC. The spectrum of the third harmonic depending on the pump power. Carrier concentration and induced field amplitude inside the nanostructure at a pump intensity of 240 GW/cm². Based on the work of I. Sinev and colleagues.²⁶⁰

types of losses. It was also shown in the work that the critical coupling regime can be achieved by changing the asymmetry parameter of the meta-atom, which should be taken into account in the design of resonant nonlinear metasurfaces. G. Zograf et al.²⁵⁹ studied the generation of higher-order odd harmonics (3,5,7,9,11) from an asymmetric silicon metasurface, shown schematically in the left panel of Fig. 21(a). The right panel of Fig. 21(a) shows the spectra of optical harmonics in the regime of excitation with 100 fs pulses and the dependence of the output power on the pump power for an optimized metasurface, using the critical coupling criterion. The dependence of the output power from pump powers in the range of 0.03 – 0.3 TW/cm² is defined by the same

law, regardless of the harmonic number, which allows a conclusion that the structure operates in a nonperturbative regime. In this paper, the transition to the nonperturbative regime is explained through the mechanism of free-carrier generation in silicon due to multiphoton absorption. J.Liu et al.¹¹⁹ studied asymmetric silicon metasurfaces with T-shaped meta-atoms, shown in Fig. 21(b). A record-high Q factor of a BIC of over 20000 was obtained in this work for a structure with 26×26 periods, achieved due to the high quality of nanolithography and special features of the structure design. In this work, the spectra of the optical second- and third-harmonic signals were measured, shown in the right panel of Fig. 21(b), and at the BIC wavelength, the harmonic signal increases by several times. I. Sinev et al.²⁶⁰ studied an asymmetric silicon metasurface for third-harmonic generation at high pump power intensities of the order of 0.3 TW/cm^2 . It was demonstrated in the work that at a pump intensity higher than 240 GW/cm^2 , self-action of a pulse occurs due to the generation of free charge carriers in the multiphoton absorption mechanism, schematically shown in the left panel of Fig. 21(c). The calculated induced field amplitude and charge carrier concentration at a peak intensity of 240 GW/cm^2 reached 3 GW/m and 10^{18} cm^{-3} , respectively, as shown in the right panel of Fig. 21(c).

Conclusion

In conclusion, bound states in the continuum have a long history in optics and radiophysics. Today, this area reaches a new level due to the fast development of the physics of metasurfaces, 2D materials, nonlinear nanophotonics, flat optics, and related directions. BICs can be observed in a wide variety of photonic structures, including metasurfaces, photonic crystal slabs, high-contrast gratings, corrugated planar waveguides and fibers, ridge waveguides, linear chains, and many others. A relatively recent discovery is a new class of BICs in Bragg resonators with an anisotropic defect layer, proposed and experimentally studied in the works.^{283–286} Today, the physics of BICs is developing in acoustics.^{20,287–289} BICs are an illustrative example of how an idea suggested in one area of physics a century ago today affects many other fields and is already used in multiple practical applications.

Acknowledgement

The authors acknowledge financial support from the Russian Foundation for Basic Research (grant no. 20-12-50314). The Authors thank A. Sadreev, E. Bulgakov, D. Maksimov, E. Bezus, D. Bykov for fruitful discussions.

References

- (1) von Neumann, J.; Wigner, E. P. Über das Verhalten von Eigenwerten bei adiabatischen Prozessen. Z. Physik **1929**, 30, 467–470.
- (2) Fonda, L.; Newton, R. G. Theory of resonance reactions. Ann. Phys. **1960**, 10, 490–515.
- (3) Stillinger, F. H.; Herrick, D. R. Bound states in the continuum. Phys. Rev. A **1975**, 11, 446.
- (4) Stillinger, F.; Weber, T. Role of electron correlation in determining the binding limit for two-electron atoms. Phys. Rev. A **1974**, 10, 1122.
- (5) Robnik, M. A simple separable Hamiltonian having bound states in the continuum. J. Phys. A: Math. Gen. **1986**, 19, 3845.
- (6) Pappademos, J.; Sukhatme, U.; Pagnamenta, A. Bound states in the continuum from supersymmetric quantum mechanics. Phys. Rev. A **1993**, 48, 3525.
- (7) Friedrich, H.; Wintgen, D. Physical realization of bound states in the continuum. Phys. Rev. A **1985**, 31, 3964.
- (8) Nöckel, J. U. Resonances in quantum-dot transport. Phys. Rev. B **1992**, 46, 15348.
- (9) Cederbaum, L. S.; Friedman, R. S.; Ryaboy, V. M.; Moiseyev, N. Conical intersections and bound molecular states embedded in the continuum. Phys. Rev. Lett. **2003**, 90, 013001.
- (10) Sadreev, A. F.; Bulgakov, E. N.; Rotter, I. Bound states in the continuum in open quantum billiards with a variable shape. Phys. Rev. B **2006**, 73, 235342.

- (11) Herrick, D. R. Construction of bound states in the continuum for epitaxial heterostructure superlattices. Physica B+C **1976**, 85, 44–50.
- (12) Stillinger, F. Potentials supporting positive-energy eigenstates and their application to semiconductor heterostructures. Physica B+ C **1976**, 85, 270–276.
- (13) Capasso, F.; Sirtori, C.; Faist, J.; Sivco, D. L.; Chu, S.-N. G.; Cho, A. Y. Observation of an electronic bound state above a potential well. Nature **1992**, 358, 565–567.
- (14) Parker, R. Resonance effects in wake shedding from parallel plates: calculation of resonant frequencies. J. Sound Vib. **1967**, 5, 330–343.
- (15) Parker, R. Resonance effects in wake shedding from parallel plates: some experimental observations. J. Sound Vib. **1966**, 4, 62–72.
- (16) Evans, D.; Levitin, M.; Vassiliev, D. Existence theorems for trapped modes. J. Fluid Mech. **1994**, 261, 21–31.
- (17) Ursell, F. Trapped modes in a circular cylindrical acoustic waveguide. Proceedings of the Royal Society of London. Series A: Mathematical and Physical Sciences **1991**, 435, 575–589.
- (18) Ursell, F. Trapping modes in the theory of surface waves. Mathematical Proceedings of the Cambridge Philosophical Society. 1951; pp 347–358.
- (19) Jones, D. The eigenvalues of $\nabla^2 u + \lambda u = 0$ when the boundary conditions are given on semi-infinite domains. Mathematical Proceedings of the Cambridge Philosophical Society. 1953; pp 668–684.
- (20) Lyapina, A.; Maksimov, D.; Pilipchuk, A.; Sadreev, A. Bound states in the continuum in open acoustic resonators. J. Fluid Mech. **2015**, 780, 370–387.
- (21) Marinica, D.; Borisov, A.; Shabanov, S. Bound states in the continuum in photonics. Phys. Rev. Lett. **2008**, 100, 183902.

- (22) Bulgakov, E. N.; Sadreev, A. F. Bound states in the continuum in photonic waveguides inspired by defects. Phys. Rev. B **2008**, 78, 075105.
- (23) Callan, M.; Linton, C. M.; Evans, D. V. Trapped modes in two-dimensional waveguides. J. Fluid Mech. **1991**, 229, 51–64.
- (24) Pagneux, V. Dynamic Localization Phenomena in Elasticity, Acoustics and Electromagnetism; Springer, Vienna: Wien, Austria, 2013; pp 181–223.
- (25) Cobelli, P. J.; Pagneux, V.; Maurel, A.; Petitjeans, P. Experimental study on water-wave trapped modes. J. Fluid Mech. **2011**, 666, 445–476.
- (26) Hsu, C. W.; Zhen, B.; Stone, A. D.; Joannopoulos, J. D.; Soljačić, M. Bound states in the continuum. Nat. Rev. Mater. **2016**, 1, 16048.
- (27) Sadreev, A. F. Interference traps waves in open system: Bound states in the continuum. Rep. Prog. Phys. **2021**,
- (28) Azzam, S. I.; Kildishev, A. V. Photonic bound states in the continuum: from basics to applications. Adv. Opt. Mater. **2021**, 9, 2001469.
- (29) Koshelev, K.; Bogdanov, A.; Kivshar, Y. Meta-optics and bound states in the continuum. Sci. Bull. **2019**, 64, 836–842.
- (30) Koshelev, K.; Bogdanov, A.; Kivshar, Y. Engineering with bound states in the continuum. Optics and Photonics News **2020**, 31, 38–45.
- (31) Plotnik, Y.; Peleg, O.; Dreisow, F.; Heinrich, M.; Nolte, S.; Szameit, A.; Segev, M. Experimental observation of optical bound states in the continuum. Phys. Rev. Lett. **2011**, 107, 183901.
- (32) Kazarinov, R.; Sokolova, Z.; Suris, R. Planar distributed-feedback optical resonators. Sov. Phys.—Tech. Phys. **1976**, 21, 130–136.

- (33) Vincent, P.; Neviere, M. Corrugated dielectric waveguides: A numerical study of the second-order stop bands. Appl. Phys. **1979**, 20, 345–351.
- (34) Vincent, P.; Neviere, M. Corrugated dielectric waveguides: A numerical study of the second-order stop bands. Appl. Phys. **1979**, 20, 345–351.
- (35) Paddon, P.; Young, J. F. Two-dimensional vector-coupled-mode theory for textured planar waveguides. Phys. Rev. B **2000**, 61, 2090–2101.
- (36) Inoue, M.; Ohtaka, K.; Yanagawa, S. Light scattering from macroscopic spherical bodies. II. Reflectivity of light and electromagnetic localized state in a periodic monolayer of dielectric spheres. Phys. Rev. B **1982**, 25, 689.
- (37) Sakoda, K. Optical transmittance of a two-dimensional triangular photonic lattice. Phys. Rev. B **1995**, 51, 4672.
- (38) Sakoda, K. Transmittance and Bragg reflectivity of two-dimensional photonic lattices. Phys. Rev. B **1995**, 52, 8992.
- (39) Shipman, S. P.; Venakides, S. Resonant transmission near nonrobust periodic slab modes. Phys. Rev. E **2005**, 71, 026611.
- (40) Bonnet, E.; Letartre, X.; Cachard, A.; Tishchenko, A.; Parriaux, O. High resonant reflection of a confined free space beam by a high contrast segmented waveguide. Opt. Express **2002**, 35, 1025–1036.
- (41) Yablonskii, A.; Muljarov, E.; Gippius, N.; Tikhodeev, S.; Ishihara, T. Optical properties of polaritonic crystal slab. Phys. Status Solidi A **2002**, 190, 413–419.
- (42) Henry, C.; Kazarinov, R.; Logan, R.; Yen, R. Observation of destructive interference in the radiation loss of second-order distributed feedback lasers. IEEE J. Quantum Elect. **1985**, 21, 151–154.

- (43) Avrutskii, I. A.; Golubenko, G. A.; Sychugov, V. A.; Tishchenko, A. V. Spectral and laser characteristics of a mirror with a corrugated waveguide on its surface. Sov. J. Quantum Electron. **1986**, 16, 1063–1065.
- (44) Robertson, W.; Arjavalingham, G.; Meade, R.; Brommer, K.; Rappe, A. M.; Joannopoulos, J. Measurement of photonic band structure in a two-dimensional periodic dielectric array. Phys. Rev. Lett. **1992**, 68, 2023.
- (45) Pacradouni, V.; Mandeville, W. J.; Cowan, A. R.; Paddon, P.; Young, J. F.; Johnson, S. R. Photonic band structure of dielectric membranes periodically textured in two dimensions. Phys. Rev. B **2000**, 62, 4204–4207.
- (46) Zhen, B.; Hsu, C. W.; Lu, L.; Stone, A. D.; Soljačić, M. Topological nature of optical bound states in the continuum. Phys. Rev. Lett. **2014**, 113, 257401.
- (47) Bulgakov, E.; Maksimov, D.; Semina, P.; Skorobogatov, S. Propagating bound states in the continuum in dielectric gratings. JOSA B **2018**, 35, 1218–1222.
- (48) Jin, J.; Yin, X.; Ni, L.; Soljačić, M.; Zhen, B.; Peng, C. Topologically enabled ultrahigh-Q guided resonances robust to out-of-plane scattering. Nature **2019**, 574, 501–504.
- (49) Hsu, C. W.; Zhen, B.; Lee, J.; Chua, S.-L.; Johnson, S. G.; Joannopoulos, J. D.; Soljačić, M. Observation of trapped light within the radiation continuum. Nature **2013**, 499, 188.
- (50) Fujita, T.; Sato, Y.; Kuitani, T.; Ishihara, T. Tunable polariton absorption of distributed feedback microcavities at room temperature. Phys. Rev. B **1998**, 57, 12428.
- (51) Yablonskii, A. L.; Muljarov, E. A.; Gippius, N. A.; Tikhodeev, S. G.; Fujita, T.; Ishihara, T. Polariton effect in distributed feedback microcavities. J. Phys. Soc. Jpn. **2001**, 70, 1137–1144.
- (52) Fan, S.; Joannopoulos, J. Analysis of guided resonances in photonic crystal slabs. Phys. Rev. B **2002**, 65, 235112.

- (53) Tikhodeev, S. G.; Yablonskii, A.; Muljarov, E.; Gippius, N. A.; Ishihara, T. Quasiguided modes and optical properties of photonic crystal slabs. Phys. Rev. B **2002**, 66, 045102.
- (54) Ochiai, T.; Sakoda, K. Dispersion relation and optical transmittance of a hexagonal photonic crystal slab. Phys. Rev. B **2001**, 63, 125107.
- (55) Volya, A.; Zelevinsky, V. Non-Hermitian effective Hamiltonian and continuum shell model. Phys. Rev. C **2003**, 67, 054322.
- (56) Dicke, R. H. Coherence in spontaneous radiation processes. Phys. Rev. **1954**, 93, 99.
- (57) Mlynek, J. A.; Abdumalikov, A. A.; Eichler, C.; Wallraff, A. Observation of Dicke superradiance for two artificial atoms in a cavity with high decay rate. Nat. Commun. **2014**, 5, 1–6.
- (58) Cao, H.; Wiersig, J. Dielectric microcavities: Model systems for wave chaos and non-Hermitian physics. Rev. Mod. Phys. **2015**, 87, 61.
- (59) Kittel, C.; McEuen, P.; McEuen, P. Introduction to solid state physics; Wiley: New York, 1996; Vol. 8.
- (60) Gao, X.; Hsu, C. W.; Zhen, B.; Lin, X.; Joannopoulos, J. D.; Soljačić, M.; Chen, H. Formation mechanism of guided resonances and bound states in the continuum in photonic crystal slabs. Sci. Rep. **2016**, 6, 31908.
- (61) Bulgakov, E. N.; Maksimov, D. N. Avoided crossings and bound states in the continuum in low-contrast dielectric gratings. Phys. Rev. A **2018**, 98, 053840.
- (62) Monticone, F.; Alu, A. Embedded photonic eigenvalues in 3D nanostructures. Phys. Rev. Lett. **2014**, 112, 213903.
- (63) Liberal, I.; Engheta, N. Nonradiating and radiating modes excited by quantum emitters in open epsilon-near-zero cavities. Sci. Adv. **2016**, 2, e1600987.

- (64) Deriy, I.; Toftul, I.; Petrov, M.; Bogdanov, A. Bound States in the Continuum in Compact Acoustic Resonators. Phys. Rev. Lett. **2022**, 128, 084301.
- (65) Lepetit, T.; Kanté, B. Controlling multipolar radiation with symmetries for electromagnetic bound states in the continuum. Phys. Rev. B **2014**, 90, 241103.
- (66) Pilipchuk, A.; Pilipchuk, A.; Sadreev, A. Bound states in the continuum in open spherical resonator. Phys. Scripta **2020**, 95, 085002.
- (67) Sadrieva, Z. F.; Belyakov, M. A.; Balezin, M. A.; Kapitanova, P. V.; Nenasheva, E. A.; Sadreev, A. F.; Bogdanov, A. A. Experimental observation of a symmetry-protected bound state in the continuum in a chain of dielectric disks. Phys. Rev. A **2019**, 99, 053804.
- (68) Yuan, L.; Lu, Y. Y. Parametric dependence of bound states in the continuum on periodic structures. Phys. Rev. A **2020**, 102, 033513.
- (69) Gao, X.; Zhen, B.; Soljacic, M.; Chen, H.; Hsu, C. W. Bound states in the continuum in fiber Bragg gratings. ACS Photonics **2019**,
- (70) Wang, Y.; Song, J.; Dong, L.; Lu, M. Optical bound states in slotted high-contrast gratings. JOSA B **2016**, 33, 2472–2479.
- (71) Kodigala, A.; Lepetit, T.; Gu, Q.; Bahari, B.; Fainman, Y.; Kanté, B. Lasing action from photonic bound states in continuum. Nature **2017**, 541, 196.
- (72) Ndangali, R. F.; Shabanov, S. V. Electromagnetic bound states in the radiation continuum for periodic double arrays of subwavelength dielectric cylinders. J. Math. Phys. **2010**, 51, 102901.
- (73) Bulgakov, E. N.; Sadreev, A. F. Bloch bound states in the radiation continuum in a periodic array of dielectric rods. Phys. Rev. A **2014**, 90, 053801.
- (74) Jackson, J. D. Classical electrodynamics; 2nd ed.; Wiley: New York, NY, 1975.

- (75) Grahn, P.; Shevchenko, A.; Kaivola, M. Electromagnetic multipole theory for optical nano-materials. New J. Phys. **2012**, 14, 093033.
- (76) Miroshnichenko, A. E.; Evlyukhin, A. B.; Yu, Y. F.; Bakker, R. M.; Chipouline, A.; Kuznetsov, A. I.; Luk'yanchuk, B.; Chichkov, B. N.; Kivshar, Y. S. Nonradiating anapole modes in dielectric nanoparticles. Nat. Commun. **2015**, 6, 1–8.
- (77) Yang, Y.; Bozhevolnyi, S. I. Nonradiating anapole states in nanophotonics: from fundamentals to applications. Acs. Sym. Ser. **2019**, 30, 204001.
- (78) Poshakinskiy, A. V.; Poddubny, A. N. Optomechanical Kerker Effect. Phys. Rev. X **2019**, 9, 011008.
- (79) Shamkhi, H. K.; Baryshnikova, K. V.; Sayanskiy, A.; Kapitanova, P.; Terekhov, P. D.; Karabchevsky, A.; Evlyukhin, A. B.; Belov, P.; Kivshar, Y.; Shalin, A. S. Transverse scattering with the generalised Kerker effect in high-index nanoparticles. Phys. Rev. Lett. **2018**, 122, 193905.
- (80) Liu, W.; Kivshar, Y. S. Generalized Kerker effects in nanophotonics and meta-optics (Invited). Opt. Express **2018**, 26, 13085–13105.
- (81) Ruan, Z.; Fan, S. Superscattering of light from subwavelength nanostructures. Phys. Rev. Lett. **2010**, 105, 013901.
- (82) Ruan, Z.; Fan, S. Design of subwavelength superscattering nanospheres. Appl. Phys. Lett. **2011**, 98, 043101.
- (83) Qian, C.; Lin, X.; Yang, Y.; Xiong, X.; Wang, H.; Li, E.; Kaminer, I.; Zhang, B.; Chen, H. Experimental observation of superscattering. Phys. Rev. Lett. **2019**, 122, 063901.
- (84) Krasikov, S.; Odit, M.; Dobrykh, D.; Yusupov, I.; Mikhailovskaya, A.; Shakirova, D.; Shcherbakov, A.; Slobozhanyuk, A.; Ginzburg, P.; Filonov, D., et al. Multipolar engineering

- of subwavelength dielectric particles for scattering enhancement. Phys. Rev. Appl. **2021**, 15, 024052.
- (85) Chen, W.; Chen, Y.; Liu, W. Singularities and Poincaré Indexes of Electromagnetic Multipoles. Phys. Rev. Lett. **2019**, 122, 153907.
- (86) Sadrieva, Z.; Frizyuk, K.; Petrov, M.; Kivshar, Y.; Bogdanov, A. Multipolar origin of bound states in the continuum. Phys. Rev. B **2019**, 100, 115303.
- (87) Bohren, C. F.; Huffman, D. R. Absorption and scattering of light by small particles.; Wiley, 1983; pp xiv, 530 p.
- (88) Mylnikov, V.; Ha, S. T.; Pan, Z.; Valuckas, V.; Paniagua-Domínguez, R.; Demir, H. V.; Kuznetsov, A. I. Lasing action in single subwavelength particles supporting supercavity modes. ACS Nano **2020**, 14, 7338–7346.
- (89) Ivchenko, E.; Pikus, G. Crystal Symmetry. In: Superlattices and Other Heterostructures.; Springer Series in Solid-State Sciences, Springer, Berlin, Heidelberg, 1995; Vol. 110.
- (90) Sakoda, K. Optical properties of photonic crystals; Springer Science & Business Media, 2004; Vol. 80.
- (91) Agranovich, V. M.; Ginzburg, V. Crystal optics with spatial dispersion, and excitons; Springer Science and Business Media, 2013; Vol. 42.
- (92) Dyakov, S. A.; Stepikhova, M. V.; Bogdanov, A. A.; Novikov, A. V.; Yurasov, D. V.; Shaleev, M. V.; Krasilnik, Z. F.; Tikhodeev, S. G.; Gippius, N. A. Photonic Bound States in the Continuum in Si Structures with the Self-Assembled Ge Nanoislands. Laser Photonics Rev. **2021**, 2000242.
- (93) Overvig, A. C.; Malek, S. C.; Carter, M. J.; Shrestha, S.; Yu, N. Selection Rules for Symmetry-Protected Bound States in the Continuum. Phys. Rev. B **2020**, 102, 035434.

- (94) Doeleman, H. M.; Monticone, F.; Hollander, W.; Alù, A.; Koenderink, A. F. Experimental observation of a polarization vortex at an optical bound state in the continuum. Nat. Photonics **2018**, 1.
- (95) Yoda, T.; Notomi, M. Generation and annihilation of topologically protected bound states in the continuum and circularly polarized states by symmetry breaking. Phys. Rev. Lett. **2020**, 125, 053902.
- (96) Bulgakov, E. N.; Maksimov, D. N. Topological bound states in the continuum in arrays of dielectric spheres. Phys. Rev. Lett. **2017**, 118, 267401.
- (97) Bykov, D. A.; Bezus, E. A.; Doskolovich, L. L. Bound states in the continuum and strong phase resonances in integrated Gires-Tournois interferometer. P. Soc. Photo-opt. Ins. **2019**, 9, 83–92.
- (98) Liu, W.; Wang, B.; Zhang, Y.; Wang, J.; Zhao, M.; Guan, F.; Liu, X.; Shi, L.; Zi, J. Circularly polarized states spawning from bound states in the continuum. Phys. Rev. Lett. **2019**, 123, 116104.
- (99) Bulgakov, E. N.; Sadreev, A. F. Bound states in the continuum with high orbital angular momentum in a dielectric rod with periodically modulated permittivity. Phys. Rev. A **2017**, 96, 013841.
- (100) Huang, C.; Zhang, C.; Xiao, S.; Wang, Y.; Fan, Y.; Liu, Y.; Zhang, N.; Qu, G.; Ji, H.; Han, J., et al. Ultrafast control of vortex microlasers. Science **2020**, 367, 1018–1021.
- (101) Bai, T.; Li, Q.; Wang, Y.; Chen, Y.; Hu, Z.-D.; Wang, J. Terahertz vortex beam generator based on bound states in the continuum. Opt. Express **2021**, 29, 25270–25279.
- (102) Wang, B.; Liu, W.; Zhao, M.; Wang, J.; Zhang, Y.; Chen, A.; Guan, F.; Liu, X.; Shi, L.; Zi, J. Generating optical vortex beams by momentum-space polarization vortices centred at bound states in the continuum. Nat. Photonics **2020**, 1–6.

- (103) Webster, M.; Pafchek, R.; Mitchell, A.; Koch, T. Width dependence of inherent TM-mode lateral leakage loss in silicon-on-insulator ridge waveguides. IEEE Photon. Technol. Lett. **2007**, 19, 429–431.
- (104) Tummidhi, R. S.; Nguyen, T.; Mitchell, A.; Koch, T. L. Anomalous losses in curved waveguides and directional couplers at “magic widths”. LEOS 2008-21st Annual Meeting of the IEEE Lasers and Electro-Optics Society. 2008; pp 521–522.
- (105) Nguyen, T. G.; Ren, G.; Schoenhardt, S.; Knoerzer, M.; Boes, A.; Mitchell, A. Ridge resonance in silicon photonics harnessing bound states in the continuum. Laser Photonics Rev. **2019**, 13, 1900035.
- (106) Bezus, E. A.; Bykov, D. A.; Doskolovich, L. L. Bound states in the continuum and high-Q resonances supported by a dielectric ridge on a slab waveguide. Photonics Res. **2018**, 6, 1084–1093.
- (107) Azzam, S. I.; Shalaev, V. M.; Boltasseva, A.; Kildishev, A. V. Formation of Bound States in the Continuum in Hybrid Plasmonic-Photonic Systems. Phys. Rev. Lett. **2018**, 121, 253901.
- (108) Liang, Y.; Koshelev, K.; Zhang, F.; Lin, H.; Lin, S.; Wu, J.; Jia, B.; Kivshar, Y. Bound states in the continuum in anisotropic plasmonic metasurfaces. Nano Lett. **2020**,
- (109) Sun, S.; Ding, Y.; Li, H.; Hu, P.; Cheng, C.-W.; Sang, Y.; Cao, F.; Hu, Y.; Alù, A.; Liu, D., et al. Tunable plasmonic bound states in the continuum in the visible range. Phys. Rev. B **2021**, 103, 045416.
- (110) Koshelev, K.; Lepeshov, S.; Liu, M.; Bogdanov, A.; Kivshar, Y. Asymmetric metasurfaces with high-Q resonances governed by bound states in the continuum. Phys. Rev. Lett. **2018**, 121, 193903.
- (111) Piper, J. R.; Fan, S. Total absorption in a graphene monolayer in the optical regime by critical coupling with a photonic crystal guided resonance. ACS Photonics **2014**, 1, 347–353.

- (112) Choi, J. M.; Lee, R. K.; Yariv, A. Control of critical coupling in a ring resonator–fiber configuration: application to wavelength-selective switching, modulation, amplification, and oscillation. Opt. Lett. **2001**, 26, 1236–1238.
- (113) Pernice, W.; Xiong, C.; Schuck, C.; Tang, H. Second harmonic generation in phase matched aluminum nitride waveguides and micro-ring resonators. Appl. Phys. Lett. **2012**, 100, 223501.
- (114) Seok, T. J.; Jamshidi, A.; Kim, M.; Dhuey, S.; Lakhani, A.; Choo, H.; Schuck, P. J.; Cabrini, S.; Schwartzberg, A. M.; Bokor, J., et al. Radiation engineering of optical antennas for maximum field enhancement. Nano Lett. **2011**, 11, 2606–2610.
- (115) Koshelev, K.; Tang, Y.; Li, K.; Choi, D.-Y.; Li, G.; Kivshar, Y. Nonlinear metasurfaces governed by bound states in the continuum. ACS Photonics **2019**, 6, 1639–1644.
- (116) Platte, W.; Sauerer, B. Optically CW-induced losses in semiconductor coplanar waveguides. IEEE T. Microw. Theory **1989**, 37, 139–149.
- (117) Makarov, S.; Kudryashov, S.; Mukhin, I.; Mozharov, A.; Milichko, V.; Krasnok, A.; Belov, P. Tuning of magnetic optical response in a dielectric nanoparticle by ultrafast photoexcitation of dense electron–hole plasma. Nano Lett. **2015**, 15, 6187–6192.
- (118) Mazurenko, D. A.; Kerst, R.; Dijkhuis, J.; Akimov, A.; Golubev, V.; Kurdyukov, D.; Pevtsov, A.; Sel’Kin, A. Ultrafast optical switching in three-dimensional photonic crystals. Phys. Rev. Lett. **2003**, 91, 213903.
- (119) Liu, Z.; Xu, Y.; Lin, Y.; Xiang, J.; Feng, T.; Cao, Q.; Li, J.; Lan, S.; Liu, J. High-Q quasi-bound states in the continuum for nonlinear metasurfaces. Phys. Rev. Lett. **2019**, 123, 253901.
- (120) Hwang, M.-S.; Lee, H.-C.; Kim, K.-H.; Jeong, K.-Y.; Kwon, S.-H.; Koshelev, K.;

- Kivshar, Y.; Park, H.-G. Ultralow-threshold laser using super-bound states in the continuum. Nat. Commun. **2021**, *12*, 1–9.
- (121) Chukhrov, A.; Krasikov, S.; Yulin, A.; Bogdanov, A. Excitation of a bound state in the continuum via spontaneous symmetry breaking. Phys. Rev. B **2021**, *103*, 214312.
- (122) Bulgakov, E.; Pichugin, K.; Sadreev, A. All-optical light storage in bound states in the continuum and release by demand. Opt. Express **2015**, *23*, 22520–22531.
- (123) Lannebère, S.; Silveirinha, M. G. Optical meta-atom for localization of light with quantized energy. Nat. Commun. **2015**, *6*, 8766.
- (124) Sadrieva, Z. F.; Sinev, I. S.; Koshelev, K. L.; Samusev, A.; Iorsh, I. V.; Takayama, O.; Malureanu, R.; Bogdanov, A. A.; Lavrinenko, A. V. Transition from Optical Bound States in the Continuum to Leaky Resonances: Role of Substrate and Roughness. ACS Photonics **2017**, *4*, 723–727.
- (125) Bulgakov, E. N.; Maksimov, D. N. Light enhancement by quasi-bound states in the continuum in dielectric arrays. Opt. Express **2017**, *25*, 14134.
- (126) Bulgakov, E. N.; Sadreev, A. F. Nearly bound states in the radiation continuum in a circular array of dielectric rods. Phys. Rev. A **2018**, *97*, 033834.
- (127) Bulgakov, E. N.; Sadreev, A. F. Transfer of spin angular momentum of an incident wave into orbital angular momentum of the bound states in the continuum in an array of dielectric spheres. Phys. Rev. A **2016**, *94*, 033856.
- (128) Bulgakov, E.; Sadreev, A. Trapping of light with angular orbital momentum above the light cone. Adv. Electromagn. **2017**, *6*, 1.
- (129) Sidorenko, M.; Sergaeva, O.; Sadrieva, Z.; Roques-Carnes, C.; Muraev, P.; Maksimov, D.; Bogdanov, A. Observation of an accidental bound state in the continuum in a chain of dielectric disks. Phys. Rev. Appl. **2021**, *15*, 034041.

- (130) Zakomirnyi, V.; Ershov, A.; Gerasimov, V.; Karpov, S.; Ågren, H.; Rasskazov, I. Collective lattice resonances in arrays of dielectric nanoparticles: a matter of size. Opt. Lett. **2019**, 44, 5743–5746.
- (131) Romano, S.; Lamberti, A.; Masullo, M.; Penzo, E.; Cabrini, S.; Rendina, I.; Mocella, V. Optical biosensors based on photonic crystals supporting bound states in the continuum. Materials **2018**, 11, 526.
- (132) Anthur, A. P.; Zhang, H.; Paniagua-Dominguez, R.; Kalashnikov, D. A.; Ha, S. T.; Maß, T. W.; Kuznetsov, A. I.; Krivitsky, L. Continuous wave second harmonic generation enabled by quasi-bound-states in the continuum on gallium phosphide metasurfaces. Nano Lett. **2020**, 20, 8745–8751.
- (133) Chen, Z.; Yin, X.; Jin, J.; Zheng, Z.; Zhang, Z.; Wang, F.; He, L.; Zhen, B.; Peng, C. Observation of miniaturized bound states in the continuum with ultra-high quality factors. Sci. Bull. **2022**, 67, 359–366.
- (134) Ishizaki, K.; Okano, M.; Noda, S. Numerical investigation of emission in finite-sized, three-dimensional photonic crystals with structural fluctuations. JOSA B **2009**, 26, 1157–1161.
- (135) Minkov, M.; Dharanipathy, U. P.; Houdré, R.; Savona, V. Statistics of the disorder-induced losses of high-Q photonic crystal cavities. Opt. Express **2013**, 21, 28233–28245.
- (136) Biberman, A.; Shaw, M. J.; Timurdogan, E.; Wright, J. B.; Watts, M. R. Ultralow-loss silicon ring resonators. Opt. Lett. **2012**, 37, 4236–4238.
- (137) Wolf, P.-E.; Maret, G. Weak localization and coherent backscattering of photons in disordered media. Phys. Rev. Lett. **1985**, 55, 2696.
- (138) Wiersma, D. S.; Bartolini, P.; Lagendijk, A.; Righini, R. Localization of light in a disordered medium. Nature **1997**, 390, 671–673.

- (139) Poddubny, A. N.; Rybin, M. V.; Limonov, M. F.; Kivshar, Y. S. Fano interference governs wave transport in disordered systems. Nat. Commun. **2012**, 3, 1–10.
- (140) Limonov, M. F.; Richard, M. Optical properties of photonic structures: interplay of order and disorder; CRC press, 2012.
- (141) Liu, C.; Rybin, M. V.; Mao, P.; Zhang, S.; Kivshar, Y. Disorder-immune photonics based on Mie-resonant dielectric metamaterials. Physical Rev. Lett. **2019**, 123, 163901.
- (142) Galisteo-López, J. F.; Ibisate, M.; Sapienza, R.; Froufe-Pérez, L. S.; Blanco, Á.; López, C. Self-assembled photonic structures. Adv. Mater. **2011**, 23, 30–69.
- (143) Astratov, V.; Adawi, A.; Fricker, S.; Skolnick, M.; Whittaker, D.; Pusey, P. Interplay of order and disorder in the optical properties of opal photonic crystals. Phys. Rev. B **2002**, 66, 165215.
- (144) Fan, S.; Villeneuve, P. R.; Joannopoulos, J. Theoretical investigation of fabrication-related disorder on the properties of photonic crystals. J. Appl. Phys. **1995**, 78, 1415–1418.
- (145) Lifshits, I.; Gredeskul, S.; Pastur, L. Introduction to the theory of disordered systems; Wiley: New York, 1988.
- (146) Ni, L.; Jin, J.; Peng, C.; Li, Z. Analytical and statistical investigation on structural fluctuations induced radiation in photonic crystal slabs. Opt. Express **2017**, 25, 5580.
- (147) Maslova, E. E.; Rybin, M. V.; Bogdanov, A. A.; Sadrieva, Z. F. Bound states in the continuum in periodic structures with structural disorder. Nanophotonics **2021**, 10, 4313–4321.
- (148) Chen, H. L.; Wang, G.; Lee, R. K. Nearly complete survival of an entangled biphoton through bound states in continuum in disordered photonic lattices. Opt. Express **2018**, 26, 33205.

- (149) Rayleigh, L. XVII. On the maintenance of vibrations by forces of double frequency, and on the propagation of waves through a medium endowed with a periodic structure. Phil. Mag. **1887**, 24, 145–159.
- (150) Elachi, C. Waves in active and passive periodic structures: A review. Proc. IEEE **1976**, 64, 1666–1698.
- (151) Suhara, T.; Nishihara, H. Integrated optics components and devices using periodic structures. IEEE J. Quantum Elect. **1986**, 22, 845–867.
- (152) Magnusson, R.; Ko, Y. H. Guided-mode resonance nanophotonics: fundamentals and applications. Nanoengineering: Fabrication, Properties, Optics, and Devices XIII. 2016; pp 1 – 13.
- (153) Chang-Hasnain, C. J.; Yang, W. High-contrast gratings for integrated optoelectronics. Adv. Opt. Photon. **2012**, 4, 379–440.
- (154) Quaranta, G.; Basset, G.; Martin, O. J. F.; Gallinet, B. Recent Advances in Resonant Waveguide Gratings. Laser Photonics Rev. **2018**, 12, 1800017.
- (155) Qiao, P.; Yang, W.; Chang-Hasnain, C. J. Recent advances in high-contrast metastructures, metasurfaces, and photonic crystals. Adv. Opt. Photon. **2018**, 10, 180–245.
- (156) Li, L. In Gratings: Theory and Numeric Applications; Popov, E., Ed.; Institut Fresnel, 2014; Chapter 13, pp 13.1–13.40.
- (157) Botten, L. C.; Craig, M. S.; McPhedran, R. C.; Adams, J. L.; Andrewartha, J. R. The Finitely Conducting Lamellar Diffraction Grating. Optica Acta: International Journal of Optics **1981**, 28, 1087–1102.
- (158) Weiss, T.; Muljarov, E. A. How to calculate the pole expansion of the optical scattering matrix from the resonant states. Phys. Rev. B **2018**, 98, 085433.

- (159) Neale, S.; Muljarov, E. A. Resonant-state expansion for planar photonic crystal structures. Phys. Rev. B **2020**, 101, 155128.
- (160) Andreani, L. C.; Gerace, D. Photonic-crystal slabs with a triangular lattice of triangular holes investigated using a guided-mode expansion method. Phys. Rev. B **2006**, 73, 235114.
- (161) Modinos, A.; Stefanou, N.; Yannopapas, V. Applications of the layer-KKR method to photonic crystals. Opt. Express **2001**, 8, 197–202.
- (162) Cotter, N. P. K.; Preist, T. W.; Sambles, J. R. Scattering-matrix approach to multilayer diffraction. J. Opt. Soc. Am. A **1995**, 12, 1097–1103.
- (163) Tishchenko, A. V. Phenomenological representation of deep and high contrast lamellar gratings by means of the modal method. Opt. Quant. Electron. **2005**, 37, 309–330.
- (164) Lalanne, P.; Hugonin, J. P.; Chavel, P. Optical Properties of Deep Lamellar Gratings : A Coupled Bloch-Mode Insight. J. Lightwave Technol. **2006**, 24, 2442–2449.
- (165) Karagodsky, V.; Chase, C.; Chang-Hasnain, C. J. Matrix Fabry–Perot resonance mechanism in high-contrast gratings. Opt. Lett. **2011**, 36, 1704–1706.
- (166) Karagodsky, V.; Chase, C.; Chang-Hasnain, C. J. Matrix Fabry–Perot resonance mechanism in high-contrast gratings. Opt. Lett. **2011**, 36, 1704–1706.
- (167) Karagodsky, V.; Chang-Hasnain, C. J. Physics of near-wavelength high contrast gratings. Opt. Express **2012**, 20, 10888–10895.
- (168) Ovcharenko, A. I.; Blanchard, C.; Hugonin, J.-P.; Sauvan, C. Bound states in the continuum in symmetric and asymmetric photonic crystal slabs. Phys. Rev. B **2020**, 101, 155303.
- (169) Bykov, D. A.; Bezus, E. A.; Doskolovich, L. L. Coupled-wave formalism for bound states in the continuum in guided-mode resonant gratings. Phys. Rev. A **2019**, 99, 063805.

- (170) Parriaux, O.; Lyndin, N. M. Modal phenomenology of arbitrarily narrow reflection from high contrast binary gratings. J. Opt. **2019**, 21, 085608.
- (171) Weiss, T.; Gippius, N. A.; Tikhodeev, S. G.; Granet, G.; Giessen, H. Derivation of plasmonic resonances in the Fourier modal method with adaptive spatial resolution and matched coordinates. J. Opt. Soc. Am. A **2011**, 28, 238–244.
- (172) Bykov, D. A.; Doskolovich, L. L. Numerical Methods for Calculating Poles of the Scattering Matrix With Applications in Grating Theory. J. Lightwave Technol. **2013**, 31, 793–801.
- (173) Whittaker, D.; Culshaw, I. Scattering-matrix treatment of patterned multilayer photonic structures. Phys. Rev. B **1999**, 60, 2610.
- (174) Krasnok, A.; Baranov, D.; Li, H.; Miri, M.-A.; Monticone, F.; Alú, A. Anomalies in light scattering. Adv. Opt. Photonics **2019**, 11, 892–951.
- (175) Blanchard, C.; Hugonin, J.-P.; Sauvan, C. Fano resonances in photonic crystal slabs near optical bound states in the continuum. Phys. Rev. B **2016**, 94, 155303.
- (176) Pietroy, D.; Tishchenko, A. V.; Flury, M.; Parriaux, O. Bridging pole and coupled wave formalisms for grating waveguide resonance analysis and design synthesis. Opt. Express **2007**, 15, 9831–9842.
- (177) Neale, S.; Muljarov, E. A. Accidental and symmetry-protected bound states in the continuum in a photonic-crystal slab: A resonant-state expansion study. Phys. Rev. B **2021**, 103, 155112.
- (178) Bulgakov, E. N.; Maksimov, D. N. Bound states in the continuum and polarization singularities in periodic arrays of dielectric rods. Phys. Rev. A **2017**, 96, 063833.
- (179) Maystre, D.; Enoch, S.; Tayeb, G. Electromagnetic theory and applications for photonic crystals; CRC press: Boca Raton, FL, 2005.

- (180) Linton, C.; McIver, P. The scattering of water waves by an array of circular cylinders in a channel. J. Eng. Math. **1996**, 30, 661–682.
- (181) Twersky, V. Multiple scattering of radiation by an arbitrary planar configuration of parallel cylinders and by two parallel cylinders. J. Appl. Phys. **1952**, 23, 407–414.
- (182) Yuan, L.; Lu, Y. Y. Propagating Bloch modes above the lightline on a periodic array of cylinders. J. Phys. B: At. Mol. Opt. Phys. **2017**, 50, 05LT01.
- (183) Yuan, L.; Lu, Y. Y. Strong resonances on periodic arrays of cylinders and optical bistability with weak incident waves. Phys. Rev. A **2017**, 95, 023834.
- (184) Kim, S.; Kim, K.-H.; Cahoon, J. F. Optical Bound States in the Continuum with Nanowire Geometric Superlattices. Phys. Rev. Lett. **2019**, 122, 187402.
- (185) Snyder, A. W.; Love, J. Optical waveguide theory; Springer Science & Business Media, 2012.
- (186) Bulgakov, E.; Sadreev, A. Trapping of light with angular orbital momentum above the light cone. Adv. Electromagn. **2017**, 6, 1–10.
- (187) Kim, S.; Cahoon, J. F. Geometric Nanophotonics: Light Management in Single Nanowires through Morphology. Accounts Chem. Res. **2019**, 52, 3511–3520.
- (188) Meade, R. D.; Devenyi, A.; Joannopoulos, J.; Alerhand, O.; Smith, D.; Kash, K. Novel applications of photonic band gap materials: Low-loss bends and high Q cavities. J. Appl. Phys. **1994**, 75, 4753–4755.
- (189) Johnson, S. G.; Fan, S.; Villeneuve, P. R.; Joannopoulos, J. D.; Kolodziejski, L. Guided modes in photonic crystal slabs. Phys. Rev. B **1999**, 60, 5751.
- (190) Fan, S.; Joannopoulos, J. D. Analysis of guided resonances in photonic crystal slabs. Phys. Rev. B **2002**, 65, 235112.

- (191) Yang, Y.; Peng, C.; Liang, Y.; Li, Z.; Noda, S. Analytical perspective for bound states in the continuum in photonic crystal slabs. Phys. Rev. Lett. **2014**, 113, 037401.
- (192) Liang, Y.; Peng, C.; Sakai, K.; Iwahashi, S.; Noda, S. Three-dimensional coupled-wave model for square-lattice photonic crystal lasers with transverse electric polarization: A general approach. Phys. Rev. B **2011**, 84, 195119.
- (193) Rybin, M. V.; Koshelev, K. L.; Sadrieva, Z. F.; Samusev, K. B.; Bogdanov, A. A.; Limonov, M. F.; Kivshar, Y. S. High-Q supercavity modes in subwavelength dielectric resonators. Phys. Rev. Lett. **2017**, 119, 243901.
- (194) Koshelev, K.; Kivshar, Y. Light trapping gets a boost. 2019.
- (195) Han, S.; Pitchappa, P.; Wang, W.; Srivastava, Y. K.; Rybin, M. V.; Singh, R. Extended Bound States in the Continuum with Symmetry-Broken Terahertz Dielectric Metasurfaces. Adv. Opt. Mater. **2021**, 9, 2002001.
- (196) Odit, M.; Koshelev, K.; Gladyshev, S.; Ladutenko, K.; Kivshar, Y.; Bogdanov, A. Observation of supercavity modes in subwavelength dielectric resonators. Adv. Mater. **2021**, 33, 2003804.
- (197) Melik-Gaykazyan, E.; Koshelev, K.; Choi, J.-H.; Kruk, S. S.; Bogdanov, A.; Park, H.-G.; Kivshar, Y. From Fano to quasi-BIC resonances in individual dielectric nanoantennas. Nano Lett. **2021**, 21, 1765–1771.
- (198) Silveirinha, M. G. Trapping light in open plasmonic nanostructures. Phys. Rev. A **2014**, 89, 023813.
- (199) Hayran, Z.; Monticone, F. Capturing broadband light in a compact bound state in the continuum. ACS Photonics **2021**, 8, 813–823.
- (200) Lepetit, T.; Akmansoy, E.; Ganne, J.-P.; Lourtioz, J.-M. Resonance continuum coupling in high-permittivity dielectric metamaterials. Phys. Rev. B **2010**, 82, 195307.

- (201) Jacobsen, R. E.; Krasnok, A.; Arslanagic, S.; Lavrinenko, A. V.; Alu, A. Boundary-Induced Embedded Eigenstate in a Single Resonator for Advanced Sensing. 2021.
- (202) Wiersig, J. Formation of long-lived, scarlike modes near avoided resonance crossings in optical microcavities. Phys. Rev. Lett. **2006**, 97, 253901.
- (203) Rybin, M.; Kivshar, Y. Optical physics: Supercavity lasing. Nature **2017**, 541, 164.
- (204) Bogdanov, A. A.; Koshelev, K. L.; Kapitanova, P. V.; Rybin, M. V.; Gladyshev, S. A.; Sadrieva, Z. F.; Samusev, K. B.; Kivshar, Y. S.; Limonov, M. F. Bound states in the continuum and Fano resonances in the strong mode coupling regime. Advanced Photonics **2019**, 1, 016001.
- (205) Chen, W.; Chen, Y.; Liu, W. Multipolar conversion induced subwavelength high-Q Kerker supermodes with unidirectional radiations. Laser Photonics Rev. **2019**, 13, 1900067.
- (206) Koshelev, K.; Kivshar, Y. Dielectric resonant metaphotonics. ACS Photonics **2020**, 8, 102–112.
- (207) Pichugin, K.; Sadreev, A. Interaction between coaxial dielectric disks enhances the Q factor. J. Appl. Phys. **2019**, 126, 093105.
- (208) Kolodny, S.; Iorsh, I. Q/V enhancement of micropillar resonator in bound states in the continuum regime. Opt. Lett. **2020**, 45, 181–184.
- (209) Gladyshev, S.; Frizyuk, K.; Bogdanov, A. Symmetry analysis and multipole classification of eigenmodes in electromagnetic resonators for engineering their optical properties. Phys. Rev. B **2020**, 102, 075103.
- (210) Bulgakov, E.; Pichugin, K.; Sadreev, A. Exceptional points in a dielectric spheroid. Phys. Rev. A **2021**, 104, 053507.
- (211) Huang, L.; Xu, L.; Rahmani, M.; Neshev, D. N.; Miroshnichenko, A. E. Pushing the limit of high-Q mode of a single dielectric nanocavity. Advanced Photonics **2021**, 3, 016004.

- (212) Yan, W.; Lalanne, P.; Qiu, M. Shape Deformation of Nanoresonator: A Quasinormal-Mode Perturbation Theory. Phys. Rev. Lett. **2020**, 125, 013901.
- (213) Singh, R.; Al-Naib, I. A.; Yang, Y.; Roy Chowdhury, D.; Cao, W.; Rockstuhl, C.; Ozaki, T.; Morandotti, R.; Zhang, W. Observing metamaterial induced transparency in individual Fano resonators with broken symmetry. Appl. Phys. Lett. **2011**, 99, 201107.
- (214) Zhang, F.; Huang, X.; Zhao, Q.; Chen, L.; Wang, Y.; Li, Q.; He, X.; Li, C.; Chen, K. Fano resonance of an asymmetric dielectric wire pair. Appl. Phys. Lett. **2014**, 105, 172901.
- (215) Fedotov, V.; Rose, M.; Prosvirnin, S.; Papasimakis, N.; Zheludev, N. Sharp trapped-mode resonances in planar metamaterials with a broken structural symmetry. Phys. Rev. Lett. **2007**, 99, 147401.
- (216) Campione, S.; Liu, S.; Basilio, L. I.; Warne, L. K.; Langston, W. L.; Luk, T. S.; Wendt, J. R.; Reno, J. L.; Keeler, G. A.; Brener, I., et al. Broken symmetry dielectric resonators for high quality factor Fano metasurfaces. ACS Photonics **2016**, 3, 2362–2367.
- (217) Vabishchevich, P. P.; Liu, S.; Sinclair, M. B.; Keeler, G. A.; Peake, G. M.; Brener, I. Enhanced second-harmonic generation using broken symmetry III–V semiconductor fano metasurfaces. ACS Photonics **2018**,
- (218) Jain, A.; Moitra, P.; Koschny, T.; Valentine, J.; Soukoulis, C. M. Electric and magnetic response in dielectric dark states for low loss subwavelength optical meta atoms. Adv. Opt. Mater. **2015**, 3, 1431–1438.
- (219) Ndao, A.; Hsu, L.; Cai, W.; Ha, J.; Park, J.; Contractor, R.; Lo, Y.; Kanté, B. Differentiating and quantifying exosome secretion from a single cell using quasi-bound states in the continuum. P. Soc. Photo-opt. Ins. **2020**, 1.
- (220) Gorkunov, M. V.; Antonov, A. A.; Kivshar, Y. S. Metasurfaces with maximum chirality empowered by bound states in the continuum. Phys. Rev. Lett. **2020**, 125, 093903.

- (221) Gorkunov, M. V.; Antonov, A. A.; Tuz, V. R.; Kupriianov, A. S.; Kivshar, Y. S. Bound States in the Continuum Underpin Near-Lossless Maximum Chirality in Dielectric Metasurfaces. Adv. Opt. Mater. **2021**, 2100797.
- (222) Overvig, A.; Yu, N.; Alù, A. Chiral quasi-bound states in the continuum. Phys. Rev. Lett. **2021**, 126, 073001.
- (223) Tittl, A.; Leitis, A.; Liu, M.; Yesilkoy, F.; Choi, D.-Y.; Neshev, D. N.; Kivshar, Y. S.; Altug, H. Imaging-based molecular barcoding with pixelated dielectric metasurfaces. Science **2018**, 360, 1105–1109.
- (224) Leitis, A.; Tittl, A.; Liu, M.; Lee, B. H.; Gu, M. B.; Kivshar, Y. S.; Altug, H. Angle-multiplexed all-dielectric metasurfaces for broadband molecular fingerprint retrieval. Sci. Adv. **2019**, 5, eaaw2871.
- (225) Foley, J. M.; Young, S. M.; Phillips, J. D. Symmetry-protected mode coupling near normal incidence for narrow-band transmission filtering in a dielectric grating. Phys. Rev. B **2014**, 89, 165111.
- (226) Foley, J. M.; Phillips, J. D. Normal incidence narrowband transmission filtering capabilities using symmetry-protected modes of a subwavelength, dielectric grating. Opt. Lett. **2015**, 40, 2637–2640.
- (227) Cui, X.; Tian, H.; Du, Y.; Shi, G.; Zhou, Z. Normal incidence filters using symmetry-protected modes in dielectric subwavelength gratings. Sci. Rep. **2016**, 6, 36066.
- (228) Doskolovich, L. L.; Bezus, E. A.; Bykov, D. A. Integrated flat-top reflection filters operating near bound states in the continuum. Photonics Res. **2019**, 7, 1314–1322.
- (229) Gentry, C. M.; Popović, M. A. Dark state lasers. Opt. Lett. **2014**, 39, 4136–4139.
- (230) Midya, B.; Konotop, V. V. Coherent-perfect-absorber and laser for bound states in a continuum. Opt. Lett. **2018**, 43, 607–610.

- (231) Ha, S. T.; Fu, Y. H.; Emani, N. K.; Pan, Z.; Bakker, R. M.; Paniagua-Domínguez, R.; Kuznetsov, A. I. Directional lasing in resonant semiconductor nanoantenna arrays. Nat. Nanotechnol. **2018**, 13, 1042.
- (232) Wu, M.; Ha, S. T.; Shendre, S.; Durmusoglu, E. G.; Koh, W.-K.; Abujetas, D. R.; Sánchez-Gil, J. A.; Paniagua-Dominguez, R.; Demir, H. V.; Kuznetsov, A. I. Room-Temperature Lasing in Colloidal Nanoplatelets via Mie-Resonant Bound States in the Continuum. Nano Lett. **2020**,
- (233) Azzam, S. I.; Chaudhuri, K.; Lagutchev, A.; Jacob, Z.; Kim, Y. L.; Shalaev, V. M.; Boltasseva, A.; Kildishev, A. V. Single and Multi-Mode Directional Lasing from Arrays of Dielectric Nanoresonators. Laser Photonics Rev. **2021**, 15, 2000411.
- (234) Muhammad, N.; Chen, Y.; Qiu, C.-W.; Wang, G. P. Optical Bound States in Continuum in MoS₂-Based Metasurface for Directional Light Emission. Nano Lett. **2021**, 21, 967–972.
- (235) Yang, J.-H.; Huang, Z.-T.; Maksimov, D. N.; Pankin, P. S.; Timofeev, I. V.; Hong, K.-B.; Li, H.; Chen, J.-W.; Hsu, C.-Y.; Liu, Y.-Y.; Lu, T.-C.; Lin, T.-R.; Yang, C.-S.; Chen, K.-P. Low-Threshold Bound State in the Continuum Lasers in Hybrid Lattice Resonance Metasurfaces. Laser Photonics Rev. **2021**, 15, 2100118.
- (236) Ignatyeva, D.; Belotelov, V. Bound states in the continuum enable modulation of light intensity in the Faraday configuration. Opt. Lett. **2020**, 45, 6422–6425.
- (237) Chernyak, A.; Barsukova, M.; Shorokhov, A.; Musorin, A.; Fedyanin, A. Bound States in the Continuum in Magnetophotonic Metasurfaces. JETP Lett. **2020**, 111, 46–49.
- (238) Zakharov, V. A.; Poddubny, A. N. Transverse magneto-optical Kerr effect enhanced at the bound states in the continuum. Phys. Rev. A **2020**, 101, 043848.
- (239) Chen, G.; Zhang, W.; Zhang, X. Strong terahertz magneto-optical phenomena based on

- quasi-bound states in the continuum and Fano resonances. Opt. Express **2019**, 27, 16449–16460.
- (240) Zhen, B.; Chua, S.-L.; Lee, J.; Rodriguez, A. W.; Liang, X.; Johnson, S. G.; Joannopoulos, J. D.; Soljačić, M.; Shapira, O. Enabling enhanced emission and low-threshold lasing of organic molecules using special Fano resonances of macroscopic photonic crystals. Proc. Natl. Acad. Sci. **2013**, 110, 13711–13716.
- (241) Sun, T.; Kan, S.; Marriott, G.; Chang-Hasnain, C. High-contrast grating resonators for label-free detection of disease biomarkers. Sci. Rep. **2016**, 6, 27482.
- (242) Wang, Y.; Ali, M. A.; Chow, E. K.; Dong, L.; Lu, M. An optofluidic metasurface for lateral flow-through detection of breast cancer biomarker. Biosens. Bioelectron. **2018**, 107, 224–229.
- (243) Meudt, M.; Bogiadzi, C.; Wrobel, K.; Görrn, P. Hybrid photonic–plasmonic bound states in continuum for enhanced light manipulation. Adv. Opt. Mater. **2020**, 8, 2000898.
- (244) Romano, S.; Zito, G.; Managò, S.; Calafiore, G.; Penzo, E.; Cabrini, S.; De Luca, A. C.; Moccia, V. Surface-Enhanced Raman and Fluorescence Spectroscopy with an All-Dielectric Metasurface. J. Phys. Chem. C **2018**, 122, 19738–19745.
- (245) Romano, S.; Zito, G.; Yépez, S. N. L.; Cabrini, S.; Penzo, E.; Coppola, G.; Rendina, I.; Moccia, V. Tuning the exponential sensitivity of a bound-state-in-continuum optical sensor. Opt. Express **2019**, 27, 18776–18786.
- (246) Wang, Y.; Han, Z.; Du, Y.; Qin, J. Ultrasensitive terahertz sensing with high-Q toroidal dipole resonance governed by bound states in the continuum in all-dielectric metasurface. P. Soc. Photo-opt. Ins. **2021**, 1.
- (247) Yesilkoy, F.; Arvelo, E. R.; Jahani, Y.; Liu, M.; Tittl, A.; Cevher, V.; Kivshar, Y.; Altug, H.

- Ultrasensitive hyperspectral imaging and biodetection enabled by dielectric metasurfaces. Nat. Photonics **2019**, 13, 390–396.
- (248) Jahani, Y.; Arvelo, E. R.; Yesilkoy, F.; Koshelev, K.; Cianciaruso, C.; De Palma, M.; Kivshar, Y.; Altug, H. Imaging-based spectrometer-less optofluidic biosensors based on dielectric metasurfaces for detecting extracellular vesicles. Nat. Commun. **2021**, 12, 1–10.
- (249) Bulgakov, E. N.; Sadreev, A. F. Bound states in photonic Fabry-Perot resonator with nonlinear off-channel defects. Phys. Rev. B **2010**, 81, 115128.
- (250) Ndangali, F. R.; Shabanov, S. V. The resonant nonlinear scattering theory with bound states in the radiation continuum and the second harmonic generation. *Active Photonic Materials* V. 2013; p 88081F.
- (251) Bulgakov, E. N.; Sadreev, A. F. Robust bound state in the continuum in a nonlinear microcavity embedded in a photonic crystal waveguide. Opt. Lett. **2014**, 39, 5212–5215.
- (252) Pichugin, K. N.; Sadreev, A. F. Frequency comb generation by symmetry-protected bound state in the continuum. JOSA B **2015**, 32, 1630–1636.
- (253) Pichugin, K.; Sadreev, A. Self-induced light trapping in nonlinear Fabry–Perot resonators. Phys. Lett. A **2016**, 380, 3570–3574.
- (254) Wang, T.; Zhang, X. Improved third-order nonlinear effect in graphene based on bound states in the continuum. Photonics Res. **2017**, 5, 629–639.
- (255) Krasikov, S.; Bogdanov, A.; Iorsh, I. Nonlinear bound states in the continuum of a one-dimensional photonic crystal slab. Phys. Rev. B **2018**, 97, 224309.
- (256) Yuan, L.; Lu, Y. Y. Excitation of bound states in the continuum via second harmonic generations. Siam J. Appl. Math. **2020**, 80, 864–880.

- (257) Deka, J.; Jha, K. K.; Menon, S.; Krishna, A. L.; Biswas, R.; Raghunathan, V. Microscopic study of resonant third-harmonic generation from amorphous silicon nanodisk arrays. Opt. Lett. **2018**, 43, 5242–5245.
- (258) Maksimov, D. N.; Bogdanov, A. A.; Bulgakov, E. N. Optical bistability with bound states in the continuum in dielectric gratings. Phys. Rev. A **2020**, 102, 033511.
- (259) Zograf, G.; Koshelev, K.; Zalogina, A.; Korolev, V.; Hollinger, R.; Choi, D.-Y.; Zuerch, M.; Spielmann, C.; Luther-Davies, B.; Kartashov, D.; Makarov, S. V.; Kruk, S. S.; Kivshar, Y. High-Harmonic Generation from Resonant Dielectric Metasurfaces Empowered by Bound States in the Continuum. ACS Photonics **2022**, 9, 567–574.
- (260) Sinev, I. S.; Koshelev, K.; Liu, Z.; Rudenko, A.; Ladutenko, K.; Shcherbakov, A.; Sadrieva, Z.; Baranov, M.; Itina, T.; Liu, J., et al. Observation of Ultrafast Self-Action Effects in Quasi-BIC Resonant Metasurfaces. Nano Lett. **2021**,
- (261) Bahari, B.; Vallini, F.; Lepetit, T.; Tellez-Limon, R.; Park, J.; Kodigala, A.; Fainman, Y.; Kante, B. Integrated and Steerable Vortex Lasers. arXiv preprint arXiv:1707.00181 **2017**,
- (262) Yu, Z.; Xi, X.; Ma, J.; Tsang, H. K.; Zou, C.-L.; Sun, X. Photonic integrated circuits with bound states in the continuum. Optica **2019**, 6, 1342–1348.
- (263) Yu, Z.; Tong, Y.; Tsang, H. K.; Sun, X. High-dimensional communication on etchless lithium niobate platform with photonic bound states in the continuum. Nat. Commun. **2020**, 11, 1–9.
- (264) Wang, Y.; Yu, Z.; Zhang, Z.; Sun, B.; Tong, Y.; Xu, J.-B.; Sun, X.; Tsang, H. K. Bound-States-in-Continuum hybrid integration of 2D platinum diselenide on silicon nitride for high-speed photodetectors. ACS Photonics **2020**, 7, 2643–2649.
- (265) Henkel, A.; Meudt, M.; Buchmüller, M.; Görrn, P. Electrically Switchable Broadband Photonic Bound States in the Continuum. arXiv preprint arXiv:2102.01686 **2021**,

- (266) Han, S.; Cong, L.; Srivastava, Y. K.; Qiang, B.; Rybin, M. V.; Kumar, A.; Jain, R.; Lim, W. X.; Achanta, V. G.; Prabhu, S. S., et al. All-Dielectric Active Terahertz Photonics Driven by Bound States in the Continuum. Adv. Mater. **2019**, 1901921.
- (267) Mikheeva, E.; Koshelev, K.; Choi, D.-Y.; Kruk, S.; Lumeau, J.; Abdeddaim, R.; Voznyuk, I.; Enoch, S.; Kivshar, Y. Photosensitive chalcogenide metasurfaces supporting bound states in the continuum. Opt. Express **2019**, 27, 33847–33853.
- (268) Gandolfi, M.; Tognazzi, A.; Rocco, D.; De Angelis, C.; Carletti, L. Near-unity third-harmonic circular dichroism driven by a quasibound state in the continuum in asymmetric silicon metasurfaces. Phys. Rev. A **2021**, 104, 023524.
- (269) Koshelev, K. L.; Sychev, S. K.; Sadrieva, Z. F.; Bogdanov, A. A.; Iorsh, I. V. Strong coupling between excitons in transition metal dichalcogenides and optical bound states in the continuum. Phys. Rev. B **2018**, 98, 161113.
- (270) Kravtsov, V. et al. Nonlinear polaritons in a monolayer semiconductor coupled to optical bound states in the continuum. Light Sci. Appl. **2020**, 9, 1.
- (271) Cao, S.; Dong, H.; He, J.; Forsberg, E.; Jin, Y.; He, S. Normal-Incidence-Excited Strong Coupling Between Excitons and Symmetry-Protected Quasi-Bound States in the Continuum in Silicon Nitride-WS₂ Heterostructures at Room Temperature. J. Phys. Chem. Lett. **2020**,
- (272) Qin, M.; Xiao, S.; Liu, W.; Ouyang, M.; Yu, T.; Wang, T.; Liao, Q. Strong coupling between excitons and magnetic dipole quasi-bound states in the continuum in WS₂-TiO₂ hybrid metasurfaces. Opt. Express **2021**, 29, 18026–18036.
- (273) Zheng, P.; Raj, P.; Mizutani, T.; Szabo, M.; Hanson, W. A.; Barman, I. Plexcitonic Quasi-Bound States in the Continuum. Small **2021**, 17, 2102596.
- (274) Zong, X.; Li, L.; Liu, Y. Photonic bound states in the continuum in nanostructured transition metal dichalcogenides for strong photon–exciton coupling. Opt. Lett. **2021**, 46, 6095.

- (275) Al-Ani, I. A. M.; As'Ham, K.; Huang, L.; Miroshnichenko, A. E.; Hattori, H. T. Enhanced Strong Coupling of TMDC Monolayers by Bound State in the Continuum. Laser Photonics Rev. **2021**, 15, 2100240.
- (276) Bernhardt, N.; Koshelev, K.; White, S.; Meng, K. W. C.; Fröch, J. E.; Kim, S.; Tran, T. T.; Choi, D.-Y.; Kivshar, Y.; Solntsev, A. Quasi-BIC Resonant Enhancement of Second-Harmonic Generation in WS₂ Monolayers. Nano Lett. **2020**,
- (277) Lochner, F. J.; George, A.; Koshelev, K.; Bucher, T.; Najafidehaghani, E.; Fedotova, A.; Choi, D.-Y.; Pertsch, T.; Staude, I.; Kivshar, Y., et al. Hybrid Dielectric Metasurfaces for Enhancing Second-Harmonic Generation in Chemical Vapor Deposition Grown MoS₂ Monolayers. ACS Photonics **2020**,
- (278) Carletti, L.; Koshelev, K.; De Angelis, C.; Kivshar, Y. Giant nonlinear response at the nanoscale driven by bound states in the continuum. Phys. Rev. Lett. **2018**, 121, 033903.
- (279) Carletti, L.; Kruk, S. S.; Bogdanov, A. A.; De Angelis, C.; Kivshar, Y. High-harmonic generation at the nanoscale boosted by bound states in the continuum. Phys. Rev. Research **2019**, 1, 023016.
- (280) Kolodny, S. A.; Kozin, V. K.; Iorsh, I. V. Enhancement of Second-harmonic Generation in Micropillar Resonator due to the Engineered Destructive Interference. JETP Lett. **2021**,
- (281) Poddubny, A. N.; Smirnova, D. A. Nonlinear generation of quantum-entangled photons from high-Q states in dielectric nanoparticles. arXiv preprint arXiv:1808.04811 **2018**,
- (282) Romano, S.; Zito, G.; Torino, S.; Calafiore, G.; Penzo, E.; Coppola, G.; Cabrini, S.; Rendina, I.; Mocella, V. Label-free sensing of ultralow-weight molecules with all-dielectric metasurfaces supporting bound states in the continuum. Photonics Res. **2018**, 6, 726–733.
- (283) Timofeev, I. V.; Maksimov, D. N.; Sadreev, A. F. Optical defect mode with tunable Q factor in a one-dimensional anisotropic photonic crystal. Phys. Rev. B **2018**, 97, 024306.

- (284) Pankin, P. S.; Maksimov, D. N.; Chen, K.-P.; Timofeev, I. V. Fano feature induced by a bound state in the continuum via resonant state expansion. Sci. Rep. **2020**, 10, 1–10.
- (285) Pankin, P.; Wu, B.-R.; Yang, J.-H.; Chen, K.-P.; Timofeev, I.; Sadreev, A. One-dimensional photonic bound states in the continuum. Commun. Phys. **2020**, 3, 1–8.
- (286) Wu, B.-R.; Yang, J.-H.; Pankin, P. S.; Huang, C.-H.; Lee, W.; Maksimov, D. N.; Timofeev, I. V.; Chen, K.-P. Quasi-Bound States in the Continuum with Temperature-Tunable Q Factors and Critical Coupling Point at Brewster’s Angle. Laser Photonics Rev. **2021**, 15, 2000290.
- (287) Tong, H.; Liu, S.; Zhao, M.; Fang, K. Observation of phonon trapping in the continuum with topological charges. Nat. Commun. **2020**, 11, 1–7.
- (288) Deriy, I.; Toftul, I.; Petrov, M.; Bogdanov, A. Bound states in the continuum in compact acoustic resonators. Phys. Rev. Lett. **2022**, 128, 084301.
- (289) Huang, S.; Liu, T.; Zhou, Z.; Wang, X.; Zhu, J.; Li, Y. Extreme sound confinement from quasibound states in the continuum. Phys. Rev. Appl. **2020**, 14, 021001.